博士論文（要約）

Numerical study on an industrial die-filling simulation by Eurelian-Lagrangian method

（オイラー-ラグランジュ法による産業用粉末
金型充填の数値シミュレーション）

姚　華秦

Acknowledgements

I would like to express my sincere gratitude to my family who have been supporting my doctoral education financially and spiritually all the time. Your encouragement have always helped me and made my 3-year college life being less struggled.

My deepest appreciation goes to Prof. Mikio Sakai for his patient guidance and professional advices. I have learnt a lot from Sakai-sensei, not only to be prudent in scientific research but also to be a kind person with charming and positive attitude. I would also like to thank the whole Sakai-lab members who are nice and supportive. You all made my doctoral life happier and brighter.

Without any of yours accompany, I could not have experienced such a wonderful time at The University of Tokyo.

Abstract

Experiments and numerical studies have been popularly performed for industrial processes. Especially for numerical approaches, recently the development of numerical method is progressing faster and faster. In chemical engineering, the requirement for using simulation to predict various processes has been growing at a quick pace. Die filling is one of the important process that is widely used in many field in chemical engineering such as food production, pharmaceuticals, cosmetic, ceramics and fuel manufacture. It is the first step to produce a final tablet product. This Ph.D. thesis will be focusing on applying numerical simulations so called the Advanced DEM-CFD method on die filling process with many kinds of calculation conditions and discussing the validation and verification tests by showing the comparison between calculated results and experimental results. A detailed introduction and explanation of our numerical method will also be included. Through this series of study, the understanding of die filling process as well as the numerical modeling will be deepened. Our approach has made a substantial progress in powder technique and chemical engineering.

Table of Contents

iv

List of figures

List of tables

Chapter 1   Introduction

1.1.   Background of die filling system and its application

Die filling is a popular process in material engineering and chemical engineering. It is a process that the granules are delivered and dropped into a die through a feed shoe moving above the manufacture tablets [1] , see Fig. 1-1. This is the first stage for a complete tablet producing series. After the die is fully filled with designed particles, the powder is transferred through the die as a whole. The die can be moved for compaction stage, which will be compressed by machines to form a solid body and stick the materials together. After that, the process will be followed by powder ejection, sintering, and finally it will be properly sized [2]. This is a dynamic process that is involved with so many physical models and processing characteristics [3]–[7]. Three important elements are listed as: 1. the movement of solid object as the moving shoe, 2. the particle flow, and 3. the air flow. During the whole die filling process, element 1 usually does not change much since the movement of the shoe is more likely to be fixed by a same pattern all the time. However, the particle flow and the air flow are dedicated research objects that are sensitive to different phases. Initially there is a huge amount of particles packed inside the shoe. At the beginning, or primary phase of the die filling, the shoe has an initial distance from the particle deposition area, beneath which the empty die has an open mouth at the top waiting for the particle injection. Before the shoe reaches to the deposition area, the movement of the whole system is quite simple and understandable.

1

Translational motion of the shoe/wall objects is always along the table, which push forwards the particles move with it. At the same time, air is affected by the movement of the wall, although slightly, it has a macroscopic influence of the global airflow of the whole system. In the next phase, when the shoe moves over the die and the particles start to fall down, the complexity of the local die part increases. Despite of the shoe's movement, particles falling into the cavity of the die will inevitably drag the air contained inside the shoe entering the die as well. With the entrance of both particle flow and the air flow, some part of the air that is originally remained inside the die had to leak out to empty the space in the die. Some of the air release through the interspace between each single particles when the size of the particle is large enough for the air. Or the air is pushed together and generates a bubble inside the particle bed and float out as a whole.
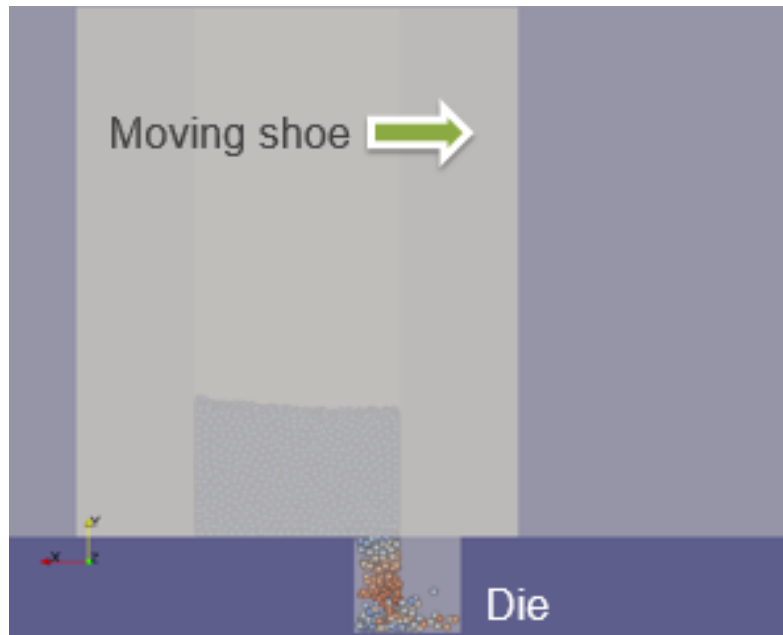
Figure 1 - 1 A typical die-shoe filling system

The comprehensive interaction among the wall, particle and air is crucial for defining and upgrading this process. In actual industrial situation, one change of each single parameter in this system could lead to a different result. On the other hand, the evaluation of the die filling system is also comprehensive due to the diversity of its system settings. Since the main production of this process is powder, the property of the particle bed is really something that producers and customers care about. The most basic evaluation standard is to identify whether the die is fully filled or not. The shoe has its own speed which is the source power of the basic die-filling mechanism. To decide the optimum speed of the shoe is hence the most fundamental factor of the system for the efficiency and the quality control. If the shoe speed is too high, there may not be enough time for the particles filling the die while the shoe is over the deposition area. In that case, the die is likely to be only partially filled which drops the quality of the outputs. If the shoe speed is too conservative, although the die is surely fully filled, the time for a single complete product could be too long to be effective [8]. Regarding the shoe speed, many studies have decided that to use the value around 0.1 m/s [8], [9]. Due to the size of a typical die, the filling duration is constrained and 0.1 m/s is basically between the results whether the die is able to be fully filled or not. The characteristic of the particle flow as well as the effect of changing particle size and density were discussed previously in Sinka's group by experiment [1], [5], [10]. In Wu's early works, the flowability characterization in die filling was also summarized [11].

According to the designer's viewpoint, a huge number of variety could be changed for particle properties, the geometry of the dies and shoes, or even the delivering mode of the whole system. The initially packed particles size may not be consistent, meaning that the kind of particle may not be the same one. Throughout the die filling researches, the particle segregation has possessed a large part of the studies [12]–[20]. Both experiments and simulations were conducted for the understanding of the particle segregation and distributions. Some of those system used not only the typical die filling setup, but introduced a rotary tablet press to test the criticisms for the empirical equations [19], [21], [22]. The tablet manufacturing has always been interested in the researchers [23], by studying which the better strategies are found out for monitoring[24], minimize the deformation or damage[25], [26], as well as the record the residence time distribution [27], [28] during the compression.

This process is widely applied in pharmaceutical industry [20], [29]–[33], such as the tablet filling process mentioned above, where tiny pharmaceutical particles were packed in the first place. In powder metallurgy [8], die filling process is used widely for manufacturing. Food production [34] is a large field for the application of die filling system. All kinds of plastic made container for such as vegetables, yogurt, drinks, egg packs are designed by the die filling process. This field concentrates mostly on the shape of the die so that their product could correspond to. Cosmetic packaging is also an interesting and highly involved industry that die filling

plays an important role in, for instance the production of lipstick or foundation make-up. Fuel fabrication is another metallurgy application which involves die filling process [35]–[37]. In a nuclear power plant [38]–[40], the power source or the fuel is manufactured into the shape of small pellet which then will be composed and assembled to be a fuel rod inserting into the reactor core. Throughout the enrichment process, Uranium dioxide is obtained in the shape of yellow powder after a series of process like dewatering, calcinations and drying. These fine particles will be delivered and pressed via the die filling system.

Experiments have been conducted for die filling study [41]–[43]. Particle sizes, blender characterization and the thermal performance were tested throughout these studies. Among previous experimental researches, the air effect has been found to be considerable especially for fine particle systems [44]. A common case for the particle deposition is by letting the granules falling inside the die at the certain position by gravity, despite of which, the suction force was examined and the results were compared with gravity fill [21], [45]. The relation between shoe velocity and fill ratio was discussed in both of the cases. Recently, with the development of the numerical method as well as the newer and newer generation of the CPU power, the study in die-shoe filling systems is not only popular in the experimental level, the research of validation tests for various numerical approaches has been brought to forth vastly.

1.2. Development of numerical simulation

During such process when fine particles drop inside the die cavity, these large number of particles are typically involved in the interactions with air as a continuous fluid, moving wall boundaries and particle themselves. Practically, tablet manufacturing requires precise controls and frequent changes of the equipment due to its delicate and complicated die geometries. Therefore one of the greatest interests in the study of die filling process is using numerical method to reproduce the whole procedure accurately and efficiently. Computer aided die filling simulation could date back to 1989 where linear programming was used [46]. To meet the requirements of the growing attention on particulate flow, a considerable number of researchers have developed their numerical approaches based on the famous Lagrangian numerical simulation that is proposed by Cundall and Strank [47]. A simple model is established by introducing springs, dash-pots and a slider to represent the contact forces on solid phase, also known as the discrete element method (DEM). It is capable of modelling the mechanical behaviors of individual solid object in a bunch of particles with a shape of disk or sphere and thus become a dominant approach for studying particulate movement [48]. Originating from Cundall and Strack's model, DEM is widely applied in powder technology [9], [49], [6], [50], [16]. It can even be applied in food industry. Some interesting studies discussed the impact damage using apple as an example [51], [52]. By coupling DEM with computational fluid dynamics (CFD), two-phase flow problems are able to be simulated on a more extensive field. It is based on the local volume

averaged Navier-Stokes equations. The finite volume description of DEM coupling with CFD was proposed by Tsuji et al. in [53]. While the point information of particles is averagely collected inside Eulerian grids, these amount of particles is still microscopic in each grid compared to the whole system[54], [55]. Thus, this technique has been positively applied on the examination of the fluidized bed behaviors [55]–[58].

From the progress and evolution of the numerical simulation viewpoint, we can easily find its developing trajectory. The numerical codes have become more and more powerful. The fidelity against the actual problems becomes more and more realistic. At first, people use experiments to collect empirical equations to constitute the modeling and simplify the algorithmic volume of the code. From the simple phase flow problems for instance the solid particle phase [59]–[61] to two-fluid problems and multi-phase problems [62]–[64], namely, particle flow considering the air flow, from 2D problems [9], [14], [18] to 3D problems [65]–[68], the numerical approach is getting powerful every academic year [69]. However there are still some ladder steps remaining for the institutes and laboratories to overcome. One of those difficulties are modeling of the wall boundary. In DEM-CFD method, the particle phase DEM is coupled with direct numerical simultaions (DNS) or LES approaches in CFD model. The information of those particles is transferred through the continuum grids by interpolation. The grids generation is always a key point for optimization. The refinement of the grid

is a topic that every CFD solver needs to consider along with the particle size and scale of the calculation domain.

The Lagrangian-Eulerian approach is famous for the multiphase coupling [70], [71]. Typically, the computational grid is constructed by mesh-based grids, so called the grids-coupled method, in which the grids information are shared between the DEM and CFD. In that case, the refinement of the grid needs to take special care given the fact that once the CFD grid is smaller than the average size of the particles, the mapped physical space may have unrealistic value for the solid volume fraction [72]. One method to generate the grid and deal with the particle information is address as grid-independent transfer scheme [73], which uses a Gaussian kernel function specifying a weighted spatial distribution that is projected to be CFD grids. In this study, the Lagrangian grids are generated by Signed Distance Function (SDF) [74]–[77]. It allows user to build 3D model on CAD software and directly generates grids by giving a completely triangulated geometry. The previous study of SDF in our group by Basinskas was to apply the SDF upon DEM, which is named as DEM/SDF [78], [79]. In those scenarios, the DEM/SDF method were tested under the industrial blender and ribbon mixer. Both the systems are popular in chemical engineering yet with complicated geometries and rapidly moving boundaries. The validation test was also done in the die filling system by Tsunazawa [80], where complicated geometries inside the die, by equipping irregular shape of obstacles, its adequacy has been fully proven. An alternative method for arbitrary die shape modeling is

to use traditional mesh-based model [81] with Finite Element Analysis. In that study, the algorithm was much more complicated than SDF. The basic concept of SDF is to construct a scalar field based on interface Ψ between the solid object and the fluid. Once Ψ is established, exterior Ψ^+ and interior Ψ^- can be determined to easily obtain the volume fraction of each grids. With this technique being applied, the coupling between DEM and CFD can be advanced into a new level of state that the movement of the boundary can easily be modeled as well as its interactions with particles.

One of the difficulty about the moving boundary is that it is difficult to model the interaction between the moving wall and the fluid along the staggered grids. The moving wall, as a boundary is not regarded in the Eulerian meshes. One example of considering the moving boundary is in direct numerical simulation (DNS) [82]–[84] for three dimensional wall-bounded flows. By using DNS, the boundary movement and its location can be precisely predicted inside the staggered grid, which by the way, the size of the object, or to say the size of the Eulerian mesh should be sufficiently enough for the resolution of the curve of the boundary shape [85]. For decades, the flow characteristics are interested by the majority of the fluid dynamics researchers. Material and literature for studying channel flow [86], [87] and bubbly flow [88], [89] have being deeply discussed. Nowadays, the direct numerical simulation development has come to a new stage where the turbulent flow [90]–[93] and multiphase flow [94], [95] started to become an in-depth study, such as the energy discussion about heat transfer and flame

9

propagation with emitted radiant energy. Cut cell mesh generation [96] is an example of modeling the moving boundary along the Cartesian grids [97], [98]. The idea of cut cell method is to intersect the solid-fluid interface even if this interface is inside a cell and generate small sub-cells [99]. In that case, the resolution of the interface could be high but on the contrary, dealing with 3D system need extra treatment [100].

Another special technique that consider the boundary as a 'solid object' is brought out by Peskin [101] that dealing with moving boundary problems in the context of continuum fluid. In the Cartesian grids, the movement of the wall geometry is treated as a forcing-term onto the continuum flow region. A well-known method is called direct-forcing, which will be introduced in this thesis. The concept of the IBM is to project the velocity and volume of the moving solid from Lagrangian grids towards the Eulerian grids. Other than the DNS method, with the utilization of the SDF-based boundary, the DEM-CFD method can easily add on the IB model [102]–[104] and simulate the movement of the wall boundary with a huge number of individual particles tracked inside the whole calculation domain. Consequently, with the simple and efficient combination of the wall boundary modeling between SDF and IBM, we propose the Advanced DEM-CFD method for a multiphase system with a moving boundary, with all of those interactions considered.

With the completion of the Advanced DEM-CFD method, will the actual die filling process be able to reproduce for the industrial application? The

answer is surely negative. This is because the scale in the industry is much larger than it is in the laboratory. A lab-level experiment may be able to reproduce by a latest CPU calculation. An actual die filling process could involve the number of particles being hundreds of thousands larger than that of a lab-scale experiment and so will the calculation time, since the calculation time should be proportional to the number of concerned particle number in DEM. The more the particles are, the longer time the calculation will take. Accordingly, a large-scale technique is also in desperately need in numerical simulations. Not only in die filling systems, in many process in chemical engineering large-scale approach is discussed such as in a CFB with the well-known Energy Minimization Multi-scale (EMMS) theory [105], [106]. It is a heterogeneous drag model that originally proposed to study and model the behavior of a cluster in a fluidized bed [107], [108]. In EMMS model, a cluster is taken into consideration which is assemble of several individual real particles or Coarse Grain particles [109]–[111]. The idea of this model is to treat the dilute phase and dense phase inside the riser separately such that in the dilute phase only a few number of real particles are need to be considered while in the dense phase a cluster gathered by real particles is modeled as a whole large particle. It is a practical method since by doing this, a lot unnecessary information from the less-interested particles will not be saved to possess the calculation memory. However in a fluidized bed system, the dense phase may have the opportunity to be considered as a whole large spherical particle with its density and diameter being modeled properly. In die filling system, the particle flow is delivered mostly by the

11

gravity and its flow pattern is a lot more different with the particle flow in the riser. Since the shoe is moving over the deposition area of the die table, the particle flow is less likely to behave like a regular shape such as a sphere. In that case, EMMS model is limited for die filling system. As a separate note, the fore-mentioned Coarse Grain particle is a basic concept of 'scale up'. One coarse grained particle is used to represent several original particles. Although in the DEM, we cannot simply substitute the real particle by a CG particle with larger diameter. The drag force acting on small particles will not be the same as the large particles and thus the energy dissipation will not be conserved. Instead, as Sakai and Koshizuka proposed in [112], a Coarse Grain model is proposed for the kinetic energy consistency [113]. It is adaptable on DEM and therefore the Coarse Grain Model (CGM) is also applied on the Advanced DEM-CFD method. Using a coarse grain ratio l, the size of the coarse grained particle will be l times larger than the original particles and l^3 times of the volume. However the coarse grain model also has its own limitation. To adapt to the DEM-CFD method, the CFD mesh size is required to be sufficiently large enough to contain several CG particles. The coarse grain particle could not be as large as we desired. Thus, to take full advantage of this modeling, a proper calculation condition should be decided, otherwise the error will be quite large and the original system could not be reproduced (See Chapter 5). Its mechanism will be introduced in Chapter 2 Section 2.3. In Chapter 4 this numerical system will be tested under the scale of an actual die filling system.

1.3. Objectives

With the numerical progress being introduced, the objective of this PhD study is to find a way to properly simulate the actual die filling process in the industrial application by using numerical modeling. In previous subsection, we mentioned that the Advanced DEM-CFD method [114] has its own advantages to deal with particle-fluid system . Although by DEM coupling with CFD, people can simulate simple two-phase flow problems at ease, there are still some difficulties remained in the existing studies as follows:

1. 2D system is easily to be constructed however, 3D modeling is not frequently applied.
2. In DEM-CFD method, traditional mesh model is algorithmically complicated to build. Only simple geometries were tested.
3. None modeling are available in the mesh-based model. The interaction between moving wall and air is ignored, i.e., a real wall boundary is improbable to model.

The complicated algorithm and time-consuming computational model make it extreme difficult to calculate the interactions of the fluid phase especially in a moving boundary system. Therefore for the first time, the Advanced DEM-CFD method has been proposed to solve all the problems at once. The SDF-based boundary construction makes it easier to combine with the Immersed Boundary technique, by using which a moving-shoe die

filling system can be easily constructed and simulated, where all the interactions considering fluid and boundaries are realized. Further than that, an industrial scale for numerical simulation has always been a bottleneck for various approaches. With the Advanced DEM-CFD proven to be adequate, our next goal is to apply the technique to a larger scale system which is able to save much computational time and in the same time, keep the results conservative. To up-scale the system, CGM is added to our method. When a coarse graining particle is calculated, it represents a group of smaller particles while keeps the properties and interactions to be the same. A series of verification tests for the Advanced DEM-CFD method applying with Coarse Grain Model were conducted to prove its applicability.

1.4.　Outline

There are five chapters in this dissertation. The first chapter is a brief introduction of the research process, namely, die filling system, the development of the numerical method for this system and the objective of the doctoral research. In the following chapter, Chapter 2, will focus on the equations and detail about our numerical approach, including the governing equations in DEM and CFD, the modeling of the wall boundary and the large scale particle modeling CGM.

Chapter 3 and Chapter 4 will demonstrate the results of applying the Advanced DEM-CFD method onto die filling systems and discuss the about the outcomes. As a first step of this study, in Chapter 3, the concept of

Advanced DEM-CFD method was firstly brought out to simulate die filling system with air considered and wall boundary interaction fully modeled. It is a validation test for a 2-stage shaped die. Based on previous DEM/SDF study, a part of the die's shape is cut and shrunk to increase the complexity and zoom into a smaller system to observe the change in fine precision. Three test series are included with one experimental data, one simulation data obtained by DEM/SDF approach and the Advanced DEM-CFD approach. All the three tests have the same geometry and particle property for the comparison. Four groups of tests with different calculation condition were conducted to prove the adequacy. By doing so we would like to emphasize the air effect that can brought to this system and to show how it can influence the particle flow. In Chapter 4, there will be further improvement on this method where CGM is combined to upscale the system. Four test groups will be shown in this chapter with different calculation conditions such as a different shoe speed or a different geometry. Chapter 5 as the final chapter, will talks about the achieved results, a summary of works that have been done and a personal perspective of future tasks with this study.

Chapter 2　　　Methodology

By using numerical method, researches are able to reproduce the industrial process without building large test facilities or preparing all kinds of experimental material. Nowadays, the personal computer's ability is crucial for deciding the calculation capacity for numerical simulations. Its power is largely depended on the central processing unit (CPU). As a limitation of modern manufacture technique, the power of CPU may not be as powerful as researchers wanted. The calculation sometimes could be so large that even using super computer located in a few institute, running time of one test case could take more than weeks and months. The scale of the simulating cases surely will have a huge influence on the calculation time period. The larger the system, the more calculation grids will be needed to construct in the model. From a whole nuclear power plant to a small tablet, the size of the system could be variated from dozens of meters to millimeters. More than that, the grid size itself also plays an important role of the fidelity of the system. Depending on their different numerical method, the calculation process and results could end up differently. However for one established system, applying different approach could become a valuable benchmark towards one or another. No matter what kind of approach people choose, the goal of numerical simulation is to reproduce the actual or realistic problems or process on computer. Not saying that in reality, those experiments that need tested are not able to perform, it is often the case that the cost of an experiment is too much. Researches or enterprises would not like to perform

test cases by spending large amount of resources. To improve the efficiency, quality and quantity of the production from one industrial process, a large amount of test cases are required. To change one simply parameter in the test could also yield in complete different results. Adjusting the parameter and all these sensitive analysis is desired to be conducted numerically, in a form of digital data. It is easier to have access to the digital data and manage it. In an actual experiment test, only the sensors and measurement meters could sometimes be hundreds of at different locations of the device. To organizing these data, especially collecting and transforming the data makes the work complicated and redundant. The content of experiment is valuable without any doubt. It is a guidance and full with reference meaning in regard of scientific researches.

On the other hand, a huge advantage of the CAD work and numerical approach is to avoid the troublesome preparation work and post processing all the data on computer is much more convenient. The research of verification and validation tests for numerical methods is growing larger and larger in universities, institutes and industrial corporates. This trend has created chances for more and more individuals or laboratories to develop their own approach and code. The computing cost for a certain industrial process becomes as low as one can realize it through a high-end CPU equipped PC, which comparing to a real experiment event, it is acceptable for those middle sized company in the market. Therefore the developing speed is also accelerated since its viability increased for most of the

laboratories. By this fashion of research, between company and company, a collaboration pattern is also developed and through this exchange study, a boost for numerical methods appeared after expo and academic conference.

In this dissertation, the numerical method will concentrate on talking about the solid particle modeling method, Discrete Element Method, coupling with the continuous fluid modeling method, Computational Fluid Dynamics. Since this study is raising the concept of the Advanced DEM-CFD method, the advancing part including the boundary modeling and its interaction between particle phase and fluid phase will be introduced in separate sections as well.

2.1. Discrete Element Method coupling with Computational Fluid Dynamics

The Advanced DEM-CFD method was applied to perform a simulation of a gas-solid flow in die-filling. The basic governing equations for DEM-CFD was nothing more than the traditional methods that could be found in most of the related numerical approaches. This section will be introducing the basic concept of the numerical approach for DEM and CFD separately.

2.1.1 Solid phase modeling

First let us start with the particle modelling. The solid phase was modeled by the DEM. In the DEM, the motion of every single particle is governed by Newton's second law of motion as,

$$m\frac{dv}{dt} = \Sigma F_c + F_d - V_s \nabla P + F_g \qquad (1)$$

$$I\frac{d\omega}{dt} = T \qquad (2)$$

where m, v, t, F_c, F_d, V_s, P, F_g, I, ω and T represent the mass of the particle, translational velocity of the particle, time, contact force, drag force, particle volume, pressure, gravitational force, moment of inertia of the particle, rotational velocity of the particle and torque respectively. According to the equation, the total force acting on the particles is composed of the contact force between particles, drag force interacting with the fluid, force due to pressure gradient and gravitational force. The contact force can be divided into two directions, normal and tangential as the equation shows,

$$F_c = F_{C_n} + F_{C_t} \qquad (3)$$

where subscript n and t represent the normal and the tangential component. Normal component of the contact force is modeled using a spring and a dashpot, and expressed by

$$F_{C_n} = -k\delta_n - \eta v_n \qquad (4)$$

where k, η, and v represent spring constant, damping coefficient, displacement and the relative velocity of the solid particles. The damping coefficient is acquired based on the energy dissipation,

$$\eta = -2(ln\, e)\sqrt{\frac{mk}{\pi^2+(ln\, e)^2}} \qquad (5)$$

where e represents the restitution coefficient.

The tangential component of the contact force is given by

$$F_{C_t} = \begin{cases} -k\boldsymbol{\delta}_t - \eta\boldsymbol{v}_t & (|F_{C_t}|\leq\mu|F_{C_n}|) \\ -\mu|F_{C_n}|\frac{\boldsymbol{v}_t}{|\boldsymbol{v}_t|} & (|F_{C_t}|>\mu|F_{C_n}|) \end{cases} \qquad (6)$$

where μ represents friction coefficient.

The drag force acting on a solid particle is given by

$$\boldsymbol{F}_d = \frac{\beta}{1-\varepsilon}(\boldsymbol{u}_f - \boldsymbol{v})\cdot V_s \qquad (7)$$

where ε, $\boldsymbol{u}_f$, and β are the void fraction, the fluid velocity and interphase momentum transfer coefficient respectively. We use Ergun [115] and Wen-Yu [116] equations to acquire the momentum exchange coefficient. The drag force of both dilute and dense gas-solid flow can be precisely computed by the model. A void fraction of 0.8 is adopted as the boundary between these two equations in the evaluation of β. The β is given by:

$$\begin{cases} \beta_{Ergun} = 150\frac{(1-\varepsilon)^2}{\varepsilon}\frac{\mu_f}{d_s^2} + 1.75(1-\varepsilon)\frac{\rho_f}{d_s}|\boldsymbol{u}_f - \boldsymbol{v}| & (\varepsilon \leq 0.8) \\ \beta_{Wen-Yu} = \frac{3}{4}C_d\frac{\varepsilon(1-\varepsilon)}{d_s}\rho_f|\boldsymbol{u}_f - \boldsymbol{v}|\varepsilon^{-2.65} & (\varepsilon > 0.8) \end{cases} \qquad (8)$$

In Eq. (8), μ_f represents the fluid viscosity, ρ_f represents the fluid density and d_s is the solid particle diameter. C_d corresponding to the drag coefficient is obtained by the following equation,

$$C_d = \begin{cases} \frac{24}{Re_s}\left(1 + 0.15Re_s^{0.687}\right) & (Re_s \leq 1000) \\ 0.44 & (Re_s > 1000) \end{cases} \qquad (9)$$

and the dimensionless particle Reynolds number expressed as Re_s is given by the equation,

$$Re_s = \frac{|u_f-v|\varepsilon\rho_f d_s}{\mu_f} \qquad (10)$$

Since the particle considered in some of the tests are so small, the Van der Waals Force [117] in that case also needs to be taken into consideration in the DEM equations. The modeling of the cohesive force is expressed as:

$$F_{cohesive} = \frac{Ha}{24 \cdot D_0^2} \cdot d_p \quad (11)$$

where D_o and Ha represents the cut-off distance and Hamaker constant, which is evaluated by using Atomic Force Microscope. The Hamaker constant determination method can be found in [118].

The algorithm of DEM simulation is listed in Fig. 2-1. From the starting of calculation, the initial conditions are firstly read and saved, such particle diameter, particle initial velocity and angle velocity, and the position of the particle. Around each of the particle, a contact search region will be generated according to its position. Since the most expensive process is to

21

detect and calculate the contact between each particle, by separate the whole calculation domain with space boxing, the DEM calculation can be more effective. In the meantime, the particles are numbered along the boxes. With the boxing area being set, particles will be put into the separated boxes and start the contact detection. The first particle marked by boxing technique will be picked up and go through the process. If its existence is within the range of other particle or boundary, the contact force will be calculated according to $\boldsymbol{F}_c$. If the contact detection returns a negative results, the calculation of the contact force will be dismissed directly to the external force calculation such as the gravity force or the drag force from the fluid. After these calculation, the process will move to the next particle, from then, the obtained information such as position and overlap data will be updated by the translational motion and rotational motion. After all of the particle data is updated, the next round starts until the end of calculation time.

As for the limitation of the calculation time step, for the sake of stability and convergence of the differential soluation, the DEM time step is recommended to be: $\Delta t < 2\sqrt{\dfrac{m}{k_n}}$ according to Cundall and Strack's research.
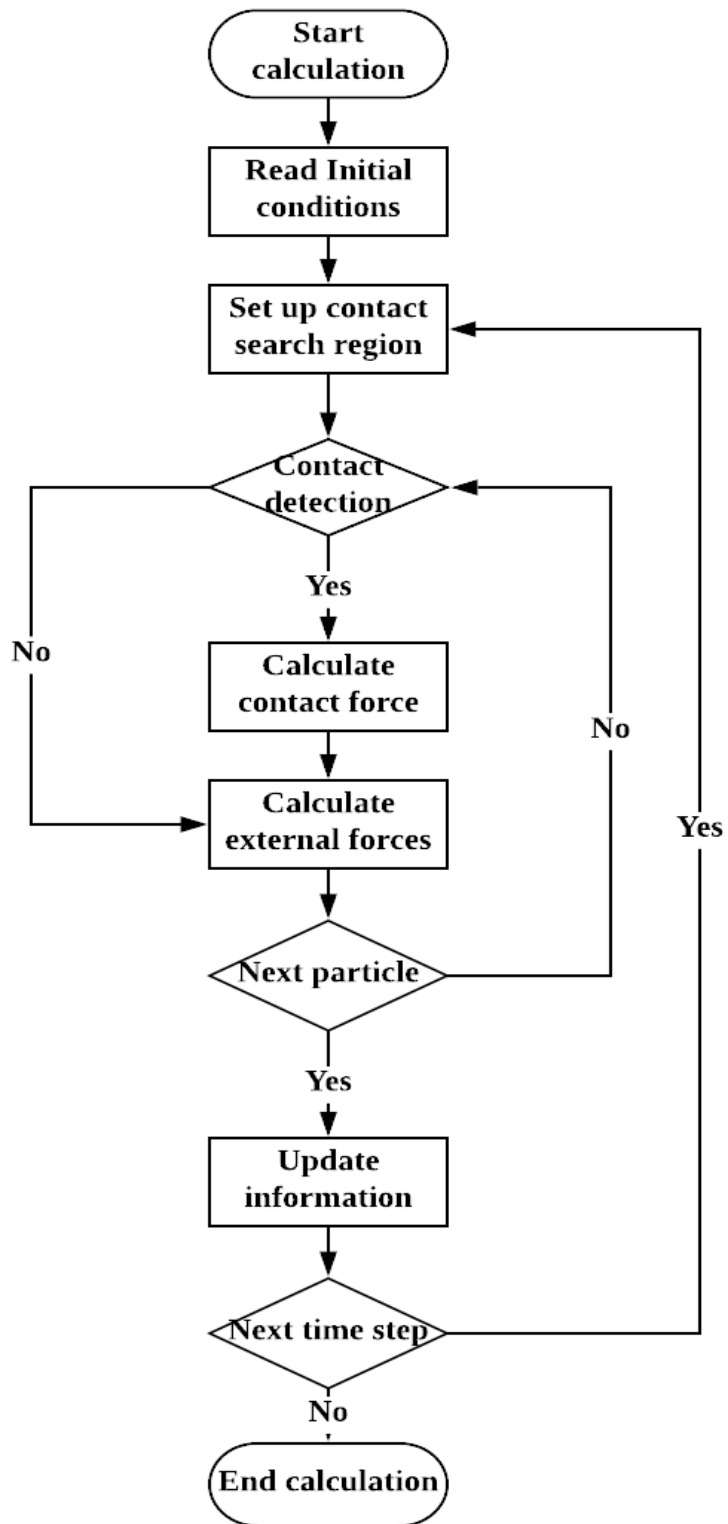
Figure 2 - 1 Algorithm of DEM

23

2.1.2 Gas phase modeling

The continuum fluid phase, or gas phase, is governed by continuity equation and Navier-Stokes equation, where local volume average technique is applied [119],

$$\frac{\partial \varepsilon}{\partial t} + \nabla \cdot \left(\varepsilon \boldsymbol{u}_f \right) = 0 \quad (12)$$

$$\frac{\partial (\varepsilon \rho_f \boldsymbol{u}_f)}{\partial t} + \nabla \cdot \left(\varepsilon \rho_f \boldsymbol{u}_f \boldsymbol{u}_f \right) = -\varepsilon \nabla P - \boldsymbol{f} + \nabla \cdot (\varepsilon \boldsymbol{\tau}) + \varepsilon \rho_f \boldsymbol{g} \quad (13)$$

where $\boldsymbol{f}$ and $\boldsymbol{\tau}$ represent the interaction between gas-solid phases and the viscous stress. $\boldsymbol{f}$ is defined according to Newton's third law of motion:

$$\boldsymbol{f} = \frac{\sum_{i=1}^{N_{grid}} \boldsymbol{F}_d}{V_{grid}} \quad (14)$$

where N_{grid} is the number of solid particles located in the local grid. V_{grid} represents the volume of one mesh in the CFD system. $\boldsymbol{F}_d$ is given by Eq. (7).

The algorithm of solving the N-S equations is shown as flow chart in Fig. 2-2, where the fractional step method is used to evaluate the fluid velocity in the staggered grids. As a first step, the initial conditions that was set through the input code were accessed and acquired. The volume fraction which can be obtained easily from the SDF-based boundary is projected from the Lagrangian wall objects onto the Eulerian fluid mesh. It is by using this combination we can accomplish this move without a complicated algorithm in the traditional mesh modeling. Next step is solving the explicit terms like

convection term and viscosity term, after this process, the first intermediate imaginary velocity $\boldsymbol{u}_f^*$ is obtained. From eq. (12), by ignoring the pressure term and the drag force term, we have the first imaginary velocity discretized for the incompressible Newtonian fluid at time step n:

$$\frac{\varepsilon\boldsymbol{u}_f^* - \varepsilon\boldsymbol{u}_f^n}{\Delta t} = -\nabla \cdot \left(\varepsilon\boldsymbol{u}_f^n\boldsymbol{u}_f^n\right) + \nu_f\nabla^2\varepsilon\boldsymbol{u}_f^n) \qquad (15)$$

where ν_f represents the kinetic viscosity of the fluid.

With the Continuity equation, the pressure Poisson's equation is expressed implicitly:

$$\nabla \cdot \left(\frac{\varepsilon}{\rho_f}\nabla P^{n+1}\right) = \frac{\nabla\varepsilon\boldsymbol{u}_f^*}{\Delta t} \qquad (16)$$

As the next step for the secondary intermediate imaginary velocity, $\boldsymbol{u}_f^{**}$ is corrected from the pressure term:

$$\frac{\varepsilon\boldsymbol{u}_f^{**} - \varepsilon\boldsymbol{u}_f^*}{\Delta t} = -\frac{\varepsilon}{\rho_f}\nabla P^{n+1} \qquad (17)$$

This $\boldsymbol{u}_f^{**}$ now is actually acquired through the traditional CFD calculation algorithm. In the Advanced DEM-CFD method, it is furtherly modeled by the Immersed Boundary Method. Adding the additional correction term $\boldsymbol{f}_{IB}$, the total velocity field can be determined which is the summation between $\boldsymbol{u}_f$ and $\boldsymbol{U}_B$, the boundary velocity. This technique will be discussed in the following sub-section 2.2.2.
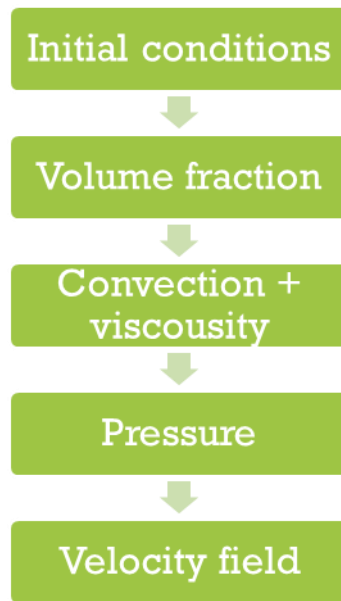
Figure 2 - 2 Fractional step for the fluid solvers.

2.2. Boundary modeling SDF and IBM

The wall boundary modeling has always been an important part in numerical simulations. In the Advanced DEM-CFD method, combination of the SDF and the IBM was employed for a moving wall boundary in die-filling. Wall boundary modeling of the Advanced DEM-CFD method is briefly addressed for solid and fluid phase as the interaction between the solid phase and the wall plus the interaction between the fluid phase and the wall. With these two mechanism applied to the traditional DEM-CFD method, the boundary modeling has become much more powerful and reliable comparing to the mesh-based boundary. Due to the different mechanism of the boundary modeling approach, this section will be divided

into two sub-sections for Signed Distance Function and Immersed Boundary Method.

2.2.1 SDF based wall boundary for solid phase

In this study, SDF was employed for creating the solid wall boundary as well as the Lagrangian meshes. The SDF is denoted as $\varphi(x)$, which is expressed as:

$$\varphi(\boldsymbol{x}) = d(\boldsymbol{x}) \cdot s(\boldsymbol{x}) \quad (18)$$

where $d(\boldsymbol{x})$ represents the minimum distance (or the nearest straight route) between the point x and the surface of the boundary structure, and $s(\boldsymbol{x})$ represents the sign of the position of the point in which case the positive indicates that x is outside the structure and a negative sign indicates that the point is outside the structure. Upon this expression, the fluid part of the system is thus outside the boundary, which will have $\varphi(\boldsymbol{x})>0$. The solid part whichever is inside the structure will be noted as $\varphi(\boldsymbol{x})<0$. And naturally wherever the points have $\varphi(\text{x})=0$, or namely the zero-level contour, are constructed as the surface of the boundary. This technique not only helped a lot building the boundary size and define the shape of the rigid body, but also has a huge advantage on combining the Immersed Boundary Method where the $\varphi(\boldsymbol{x})$ can be directly used for deciding the location or the coordinates of the immersed walls surface. In a specific case like the die filling system, the surface of the wall boundary can also be considered as the interface between

27

the two materials, namely air fluid and solid wall. At this interface, the scalar field φ satisfies the boundary condition:

$$|\nabla\varphi| = 1 \quad (19)$$

The normal vector $\boldsymbol{N}$ is thus defined as

$$\boldsymbol{N} = \nabla\varphi \quad (20)$$

Since φ is calculated through interpolation, the φ function is not to be continued in the discretized grid, which could result in the normal vector not to be 1. To normalize this mathematical problem, $\boldsymbol{N}^{SDF}$ is introduced as:

$$\boldsymbol{N}^{SDF} = \frac{\nabla\varphi}{|\nabla\varphi|} \quad (21)$$

Drag force in tangential and normal directions are calculated by the term overlap δ, which could replace the overlap term by δ^{SDF} in the DEM equations:

$$\boldsymbol{\delta}^{SDF} = (\varphi - r) \cdot \boldsymbol{N}^{SDF} \quad (22)$$

by applying $\boldsymbol{\delta}^{SDF}$, the normal and tangential components of the contact force are expressed as:

$$\boldsymbol{F}_{C_n}^{SDF} = -k\boldsymbol{\delta}^{SDF}|\nabla\varphi| - \eta\boldsymbol{v}_n \quad (23)$$

$$F_{C_t}^{SDF} = \begin{cases} -k\boldsymbol{\delta}^{SDF} - \eta\boldsymbol{v}_t & (|F_{C_t}| \le \mu |F_{C_n}|) \\ -\mu|\boldsymbol{F}_{C_n}|\frac{\boldsymbol{v}_t}{|\boldsymbol{v}_t|} & (|F_{C_t}| > \mu |F_{C_n}|) \end{cases} \quad (24)$$

where the superscript SDF in the force term indicate the overlap that has been replaced, which is between the particle and SDF based wall surface. By

applying the SDF superscript overlap, the new model is much simpler to detect the particle collisions than it is in the traditional mesh model. Because the distance is now easily represented by the point-to-surface distance, which no longer needs the check mechanism for particle-vertex, particle-edge or particle-surface. This is a simpler and more elegant way of modeling the granular flow.

2.2.2 IBM based wall boundary for gas phase

The Immersed Boundary Method is able to simulate solid-fluid interaction based on local volume fraction. In the IBM, velocity field is calculated based on volume average of the local fluid velocity and the local solid object velocity in each calculation grid. The solid-fluid interaction is evaluated based on the local volume fraction of a solid object, where the body force is proportional to the local volume fraction of the solid object. The grid size must be sufficiently smaller than the solid object. In the Advanced DEM-CFD method, the local volume of the solid object is calculated based on the SDF-generated mesh. The SDF range is usually set to be the magnitude of 10^{-4} meter, comparing the mesh size is sufficiently small. Thus the combination of the SDF and IBM makes it possible to evaluate the solid-fluid interaction of a moving object easily and accurately. The solid-fluid interface velocity is considered as a projection from solid object onto the fluid and furtherly influences the fluid velocity. Hence, the solid-fluid

interaction force given at the interface works to enforce the no-slip condition in the solid-fluid mixture grid.

In the Navier-Stokes equation, instead of calculating the fluid velocity, the velocity field $\boldsymbol{u}$ is established as,

$$\boldsymbol{u} = (1 - \alpha)\boldsymbol{u}_f + \alpha\boldsymbol{U}_B \quad (25)$$

where α and $\boldsymbol{U}_B$ represent the local volume fraction obtained by SDF and the boundary velocity. After substituting the net velocity field for fluid velocity, a correction term $\boldsymbol{f}_{IB}$ must be considered in the original Navier-Stokes equation,

$$\frac{\partial(\varepsilon\rho_f\boldsymbol{u})}{\partial t} + \nabla \cdot \left(\varepsilon\rho_f\boldsymbol{u}\boldsymbol{u}\right) = -\varepsilon\nabla P - \boldsymbol{f} + \nabla \cdot (\varepsilon\boldsymbol{\tau}) + \varepsilon\rho_f\boldsymbol{g} + \boldsymbol{f}_{IB} \quad (26)$$

where $\boldsymbol{f}_{IB} = \frac{\alpha\rho_f(\boldsymbol{U}_B - \boldsymbol{u}_f)}{\Delta t}$

Hence, to solve the corrected momentum equation again, with the secondary intermediate velocity the new velocity field can be calculated.

Fig. 2-3 illustrates an example of the Eulerian domain of one simple die filling system with the moving shoe. As shown in the zoomed view, the scalar information such as density and pressure are stored at the body center of the staggered grids. The vector information is stored at the face center of the staggered grids. During the shoe movement, the solid structure will move along the grids and immerse into the fluid part where actually the velocity and force are projected and acting on the solid-fluid interface. The volume

30

fraction information is obtained from Signed Distance Function. When α is 1, it suggests this grid is inside solid structure. When α is 0, the grid is in the exposure of air fluid. When it is between 0 and 1, the interface is appeared at this grid which makes this grid a composition of part-solid and part-fluid.
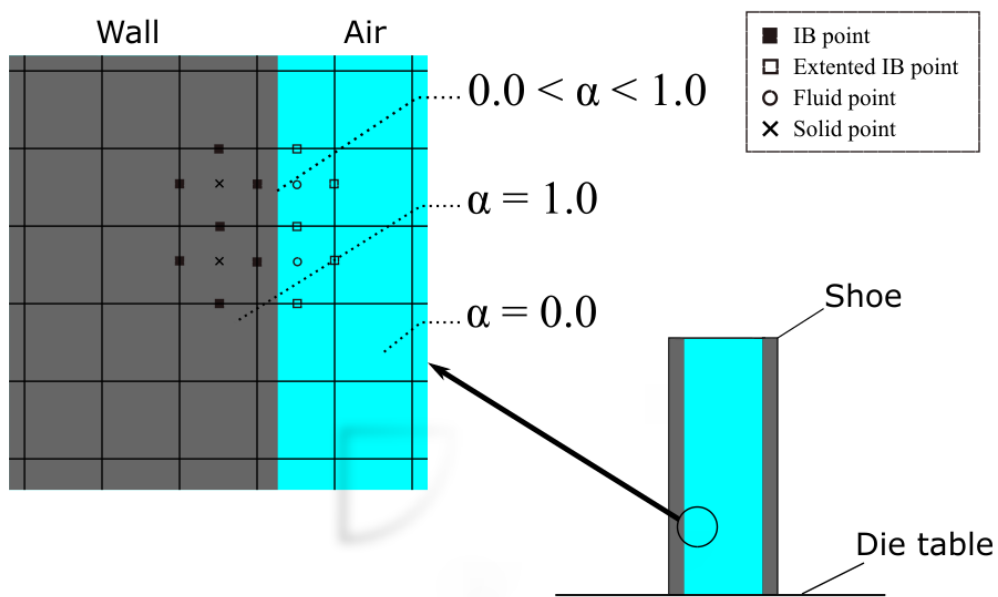

Figure 2 - 3 The Eulerian domain of die filling system.

Its spatial discretization is depended on the dimensions the system is. As for a 2D system, the discretized Pressure Poisson Equation gives 5 points in each grid with 4 vector points and one scalar point. As in the 3D system case, there will be 7 points in each block which are 6 vector points and one scalar point. Here we use the 3D case as an example of the discretization. The

spatial discretization scheme for the non-linear convective term in 3D system in **u**-component is given by:

$$\nabla(uu)_{i+\frac{1}{2},j,k} = \nabla_x(uu) + \nabla_y(vu) + \nabla_z(wu) \ \ (27)$$

in which on the right side, the first term with x-derivative can be written in finite-difference form as:

$$\nabla_x(uu) = \frac{U_{i+\frac{1}{2},j,k}u_{i+\frac{1}{2},j,k} - U_{i-\frac{1}{2},j,k}u_{i-\frac{1}{2},j,k}}{\Delta x} \ \ (28)$$

where u is obtained through linear interpolation and U is the control volume constructed by the u-velocity.

In this sub-section, three kinds of differential schemes will be mentioned as following, (1) First order upwind difference scheme. (2) Second order central difference scheme. And (3) Hybrid scheme which combines (1) and (2) with a dimensionless number Péclet number.

$$Pe = \frac{\rho u \Delta x}{\mu} \ \ (29)$$

The first order upwind difference scheme is more stable and less likely results in unphysical oscillations since it is effected by the numerical diffusion. In the Hybrid scheme [120], introducing Péclet number makes it possible to select the stability region, which is decided by the ratio between the advective transport rate to diffusive transport rate, and reasonably save computational cost. When this ratio rests at the region $-2 \leq Pe \leq 2$, the Second order central difference scheme is chosen. This means that the

convection term is less dominant than the diffusion term. Vice versa when the Péclet number lies on the region below -2 or beyond 2, meaning the convection term is more dominant than the diffusion term, First order upwind difference scheme is chosen for a more stable numerical solution.

Pressure Poisson Equation is discretized separately by a classical central difference scheme. As described in the CFD sub-section, the final velocity field is calculated by three steps, among them the pressure is obtained through the Continuity Equation, which can be discretized as follows:

$$(\nabla \cdot \boldsymbol{u}_f)_{i,j,k} = \frac{u^{n+1}_{i+\frac{1}{2},j,k} - u^{n+1}_{i-\frac{1}{2},j,k}}{\Delta x} + \frac{v^{n+1}_{i,j+\frac{1}{2},k} - v^{n+1}_{i,j-\frac{1}{2},k}}{\Delta y} + \frac{w^{n+1}_{i,j,k+\frac{1}{2}} - w^{n+1}_{i,j,k-\frac{1}{2}}}{\Delta z} = 0 \quad (30)$$

In the second step where pressure is calculated implicitly, the left hand side of the PPE is shown as:

$$\nabla \cdot (\frac{\varepsilon}{\rho} \nabla P)_{ijk} = \frac{1}{(\Delta x)^2} \varepsilon \left(\frac{P_{i+1,j,k} - P_{ijk}}{\rho_{i+\frac{1}{2},j,k}} - \frac{P_{ijk} - P_{i-1,j,k}}{\rho_{i-\frac{1}{2},j,k}} \right) + \frac{1}{(\Delta y)^2} \varepsilon \left(\frac{P_{i,j+1,k} - P_{ijk}}{\rho_{i,j+\frac{1}{2},k}} - \right.$$

$$\left. \frac{P_{ijk} - P_{i,j-1,k}}{\rho_{i,j-\frac{1}{2},k}} \right) + \frac{1}{(\Delta z)^2} \varepsilon \left(\frac{P_{i,j,k+1} - P_{ijk}}{\rho_{i,j,k+\frac{1}{2}}} - \frac{P_{ijk} - P_{i,j,k-1}}{\rho_{i,j,k-\frac{1}{2}}} \right) \quad (31)$$

and the fluid velocity can be updated by combining these two equations above. As an example of the u-component, $\boldsymbol{u}_f^{**}$ is updated:

$$\frac{\boldsymbol{u}^{**}_{f(i+\frac{1}{2},j,k)} - \boldsymbol{u}^{*}_{f(i+\frac{1}{2},j,k)}}{\Delta t} = -\frac{1}{\rho_{f(i+\frac{1}{2},j,k)}} \frac{P_{i+1,j,k} - P_{i,j,k}}{\Delta x} \quad (32)$$

In the Advanced DEM-CFD method, the Immersed Boundary Method is furtherly improved by a density scaling factor. It has been noticed that at the boundary of the interface, pressure is not properly dealt with. There is no modeling for this interface in the IBM, which could result a velocity loss due to penetration through this interface. To enforce the separation between inside and outside, a special treatment for the solid structure is utilized by adding an up-scaling factor γ to the density ρ, to improve the physical density for all the wall objects. Thus when calculating the pressure term in PPE, the density term will be conditionally replaced by $\hat{\rho}=\gamma\rho$, decided by whether the adjacent cells are wall boundary or not. In this situation, γ is the artificial scaling factor which is larger than 1, depending on the system. Usually the scaling factor is recommended to be 1000 through the past studies [102]. Through SDF-based scalar field, we can easily obtain the information of the staggered grids. Assuming we are at the position of (*i+1/2, j, k*), the density will be given as:

$$\hat{\rho}_{i+\frac{1}{2},j,k} = \begin{cases} \gamma\rho & if \ \varphi_{ijk}\leq0 \ or \ \varphi_{i+1,j,k}\leq0 \\ \rho & otherwise \end{cases} \quad (33)$$

2.3. Large-scale modeling: Coarse Grain Model

The Discrete Element Method has provided a great fashion of modeling granular systems by looking at each individual particles. Working upon a latest CPU, the amount of the particle number that under calculation simultaneously can be as large as hundreds of thousands. However the

magnitude of million numbers of particles is still likely to be considered insufficient when it comes to actual industrial process. Such a large scale system is not able to be simulated by today's computer capacity. Since the system become so large, the detail of each single particle for instance the movement or angle velocity may not be that necessary to capture. In this case, a macroscopic point of view is more preferable. Thus a large scale DEM model is developed to upgrade simulation from lab-level experiment to actual industry level, so called the Coarse Grain Model. The graphical interpretation of the Coarse Grain Model is shown in Fig. 2-4. The size of the illustrated particles is dimensionless, each case has a multiplication factor (noted as l) of the diameter to be 1, 2 and 3 respectively. The idea of CGM is using one pseudo particle with larger size to represent a group number of original particles. If the size of the CGM particle is doubled, then according to its volume, $2^3=8$ of the original particles could be represented. If the size of the CGM particle is tripled, then $3^3=27$ of the original particles could represented and so on in the similar fashion with l^3. Through this approach, the total number of particles that need to be considered can dramatically decrease and thus save the calculation time. Note that the number of every individual particle is proportional to the CPU time for DEM calculation.

As mentioned above, one large particle is modeled as a group of original particles. This large particle is addressed as a Coarse Graining particle. In Coarse Grain Model, the translational motion of CG particle is assumed to equal the average of this group of original particles. That means the velocity

and the displacement of the Coarse Grain particle is the same as that of the original particles, taking average numerical value of the group. The rotational motion of each original particle inside the Coarse Grain particle has its own center of mass with the same averaged angle velocity. As far as the contact force is concerned, an important assumption is made in the CGM that whenever a binary collision takes place between two Coarse Grain particles, the original particles which are represented by the two Coarse Grain particles also have the binary collisions simultaneously. In that way, the kinetic energy is assumed to be conserved between a CG particle and the group of original particles. That means one binary collision occurred for Coarse Grain particle with the size multiplication factor to be l, the total number of the binary collision for original particles should be l^3. This is under the estimation of the total energy for the two Coarse Grain particles is consistent to its representing group of original particles. In this fashion, the CGM can be applied on the existing DEM or the DEM-CFD method. When applying the CGM, the traditional DEM equations become:

$$m_{CGM} \frac{dv_{CGM}}{dt} = \boldsymbol{F}_{d_{CGM}} - V_{CGM} \nabla P + \sum \boldsymbol{F}_{c_{CGM}} + \boldsymbol{F}_{g_{CGM}} \quad (34)$$

$$I_{CGM} \frac{d\omega_{CGM}}{dt} = \boldsymbol{T}_{CGM} \quad (35)$$

where the subscript CGM indicates the Coarse Grain particles for replacing the original particles. Regarding the CGM functioning on the forces appeared on the equations, according to the binary collision assumption we have $\boldsymbol{F}_{CGM} = l^3 \boldsymbol{F}_{original}$.

36

For the contact force, with the same manner as DEM, it is divided into normal and tangential directions. For the normal direction, we have the contact force

$$F_{C_{n_{CGM}}} = l^3\left(-k_O \boldsymbol{\delta}_{n_{CGM}} - \eta_O \boldsymbol{v}_{n_{CGM}}\right) = l^3\left(-k_O \overline{\boldsymbol{\delta}}_{n_O} - \eta_O \overline{\boldsymbol{v}}_{n_O}\right) \quad (36)$$

where O indicates the numerical value for original system. The average value of displacement (or the overlap term) and the velocity of the original particle system by assumption replaced the Coarse Grain particles.

The tangential direction of the contact force is expressed as:

$$F_{C_{t_{CGM}}} = \begin{cases} l^3\left(-k_O \boldsymbol{\delta}_{t_{CGM}} - \eta_O \boldsymbol{v}_{t_{CGM}}\right) & \left(\left|F_{C_{t_{CGM}}}\right| \leq \mu_O \left|F_{C_{n_{CGM}}}\right|\right) \\ -l^3 \mu_O \left|F_{C_{n_{CGM}}}\right| \dfrac{\boldsymbol{v}_{t_{CGM}}}{\left|\boldsymbol{v}_{t_{CGM}}\right|} & \left(\left|F_{C_{t_{CGM}}}\right| > \mu_O \left|F_{C_{n_{CGM}}}\right|\right) \end{cases} \quad (37)$$

In the translational motion equation, the velocity of a coarse graining particle $\boldsymbol{v}_{t_{CGM}}$ is assumed to be equal to the average velocity of the modeled group of original particles $\overline{\boldsymbol{v}}_{t_O}$. With the same manner, the translational information of the Coarse Grain particles can be replaced by the value of the averaged original particle group:

$$F_{C_{t_{CGM}}} = \begin{cases} l^3\left(-k_O \overline{\boldsymbol{\delta}}_{t_O} - \eta_O \overline{\boldsymbol{v}}_{t_O}\right) & \left(\left|F_{C_{t_{CGM}}}\right| \leq \mu_O \left|F_{C_{n_{CGM}}}\right|\right) \\ -l^3 \mu_O \left|F_{C_n,O}\right| \dfrac{\boldsymbol{v}_{t_O}}{\left|\boldsymbol{v}_{t_O}\right|} & \left(\left|F_{C_{t_{CGM}}}\right| > \mu_O \left|F_{C_{n_{CGM}}}\right|\right) \end{cases} \quad (38)$$

In DEM-CFD method, drag force that modeling the interaction between particle and fluid in CGM is modeled as such:

$$F_{d,CGM} = \frac{\beta}{1-\varepsilon}(u_f - v_{CGM}) \cdot V_{s,CGM}$$

$$= l^3 \frac{\beta}{1-\varepsilon}(u_f - \bar{v}_O) \cdot \bar{V}_{s,O} \qquad (39)$$

Again, the averaged original particle translational information substitutes the CG particles, with l^3 times larger of the collision times, the kinetic energy between the two systems are conserved. Finally, the relationship of the rotational motion between two systems is as the following:

$$\frac{d\omega_{CGM}}{dt} = \frac{T_{CGM}}{I_{CGM}} = \frac{r_{CGM} \times F_{C_{t,CGM}}}{I_{CGM}} = \frac{lr_O \times l^3 F_{C_{t,O}}}{l^3 l^2 I_O} = \frac{1}{l}\frac{d\bar{\omega}_O}{dt} \quad (40)$$

in which case, the inertia momentum of a sphere is proportional to r^2. Thus in the denominator additional l^2 is multiplied
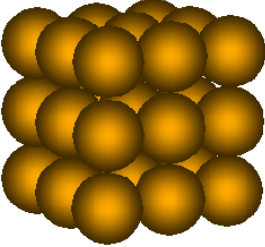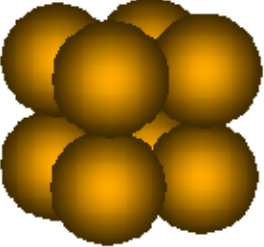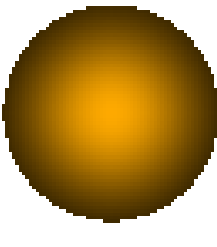
Original system	Coarse Grain Model	Coarse Grain Model
(*d*=1)	(*d*=2)	(*d*=3)

Figure 2 - 4 Coarse Grain Model

Chapter 3 Validation test using the Advanced DEM-CFD method

  As it is introduced in previous chapter, the Advanced DEM-CFD method is proposed to calculate the behaviors of granules and air fluid. Its special way of modeling boundary, i.e. the combination between SDF and IBM provides a convenient fashion to represent the movement of the wall structure with all the interaction, with particles and with air fluid, being considered. In this chapter, a complete study will be shown as the first stage of my doctoral research achievement. A validation test of our approach, which contains the experiment part and numerical simulation part. In the experiment part, the die and shoe system is provided as designed. By using a high speed camera, we captured the experiment in slow-motion view in front of the die filling system. And in the numerical simulation part, we compared the results with the experiments for every time step, mainly for their filling appearance. To demonstrate the importance of the air fluid and its effect on the particle flow, in every experiment case, one test without considering the air is added to show how the air will bring influence on this process. Three sections will be followed with firstly the experiment description, calculation conditions and finally the results and discussion.

3.1. Experiment description

NONPAREIL-108® particle (FREUND CORPORATION, Tokyo, Japan) was employed in the current study. Fig. 3-1 shows the Scanning Electron Microscope (SEM) image of the real particle. Under the microscope images, we can decide that this kind of fine particle is highly spherical with its shape. The range attached in the figure also showed that the diameter of the particle was averagely around 200 μm. The particle density was measured to be 1,379 kg/m^3, which was measured and provided by the company. In this study, the cohesive force is considered in the numerical modeling. By using Atomic Force Microscope, as shown in Fig. 3-1, the cohesive force acting on the particle was modeled and the Hamaker constant was obtained to be 4.4×10-22 J.

Fig. 3-2 and Fig. 3-3 were picture taken from the experiment. Fig. 3-2 shows the die filling system with a shoe and a gear drive system that provide mechanical energy for shoe's movement. Fig. 3-3 shows the die component used in this validation test. The powder will be initially packed inside the shoe and the particle bed will be shaken from the outside to create a flat surface inside the shoe. Next step, the gear at the end of the die table will be locked with the teeth structure of the shoe. The gear rotation speed is set to be 53 rotation per minute which through a test case we calculated its linear translational speed to be 0.10 m/s. For the other shoe speed case, the gear rotation speed is set to be 26, where it is corresponded to the linear translational speed as 0.047m/s.

40

The experiments with different initial conditions were performed as listed in Table 3-1. Dimensions of experimental device including two different die position setups is shown in Fig 3-4. Each of the setting contains a die, a shoe and a shoe table. The die is a 10 mm's cubic structure with a 5 mm's foursquare hollowed out at bottom corner of the die. The dimension of the shoe cavity is $10 \times 30 \times 10$ mm^3. There is a 2 mm thickness considered for the die table between the die and the shoe, which finally gives us a deepness of 12 mm die in the y-direction (upper stage 7 mm, lower stage 5 mm). We observed the particle behavior in die filling, where the parameter were shoe speed and die position. All the experimental tests are exposed to room air at normal temperature and pressure. Powder injection process was recorded using high speed camera FASTCAM Mini WX 100 (PHOTRON, Tokyo, Japan).
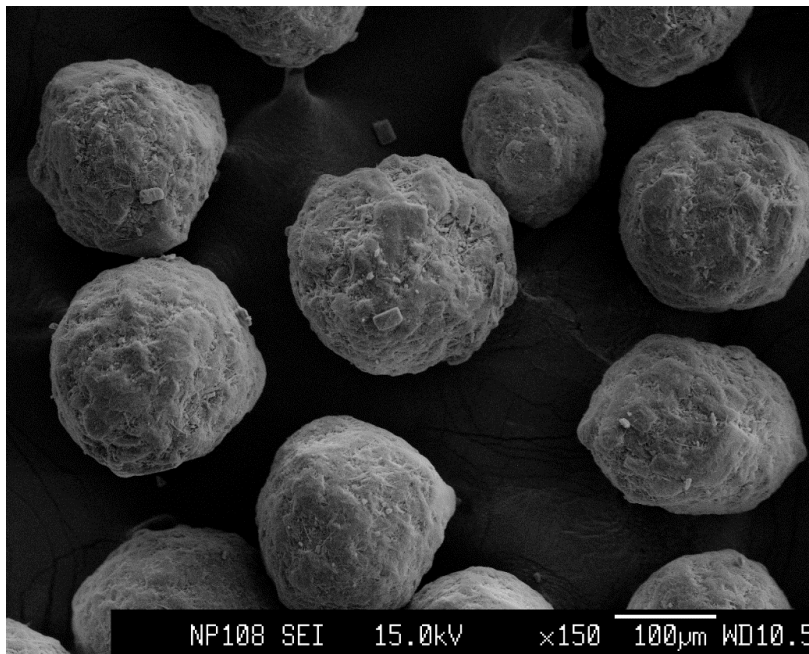

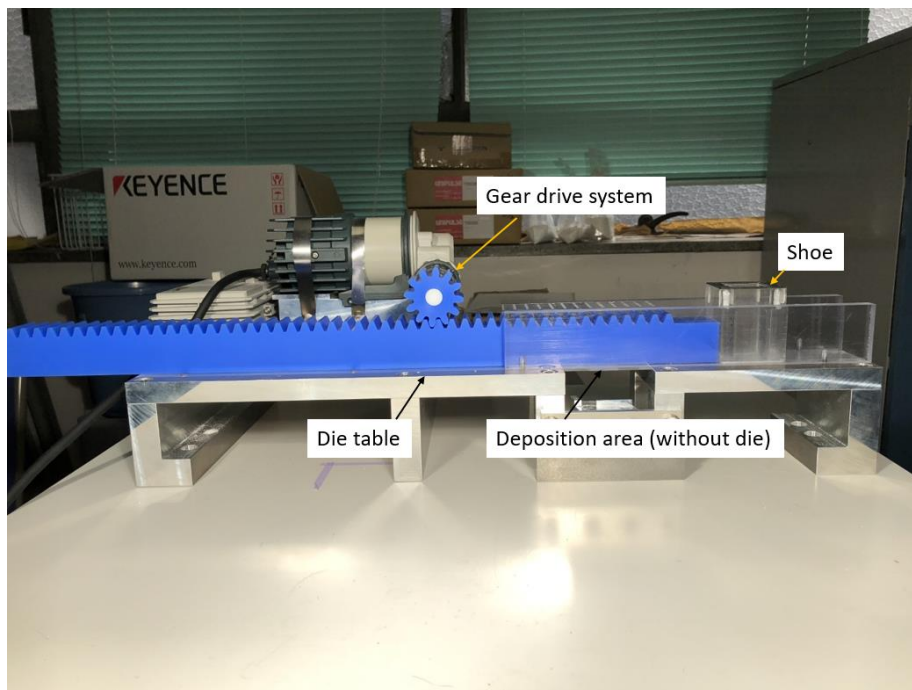Figure 3 - 1 SEM image of NONPAREIL-108® particle

41

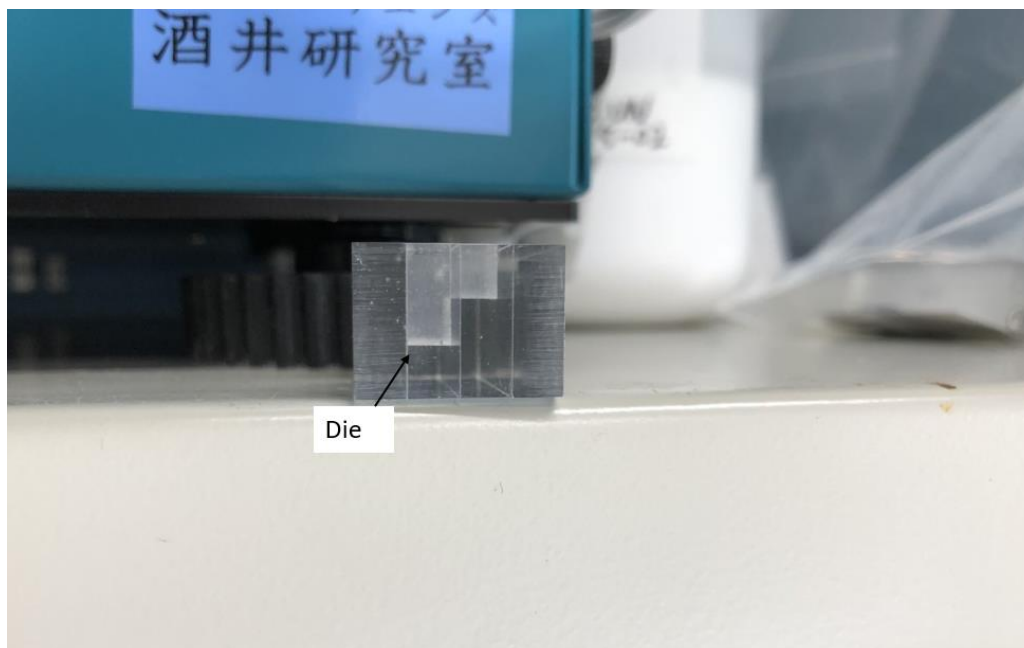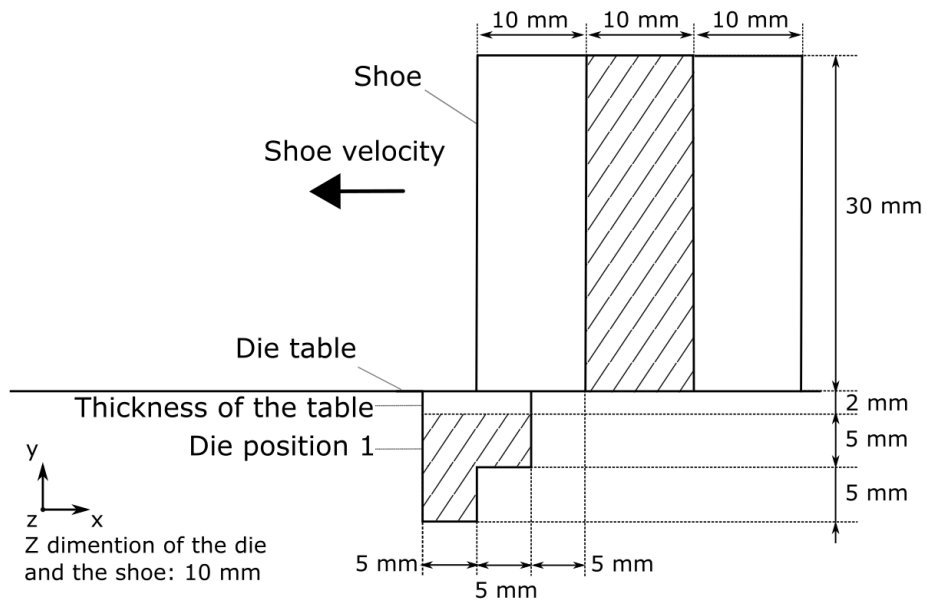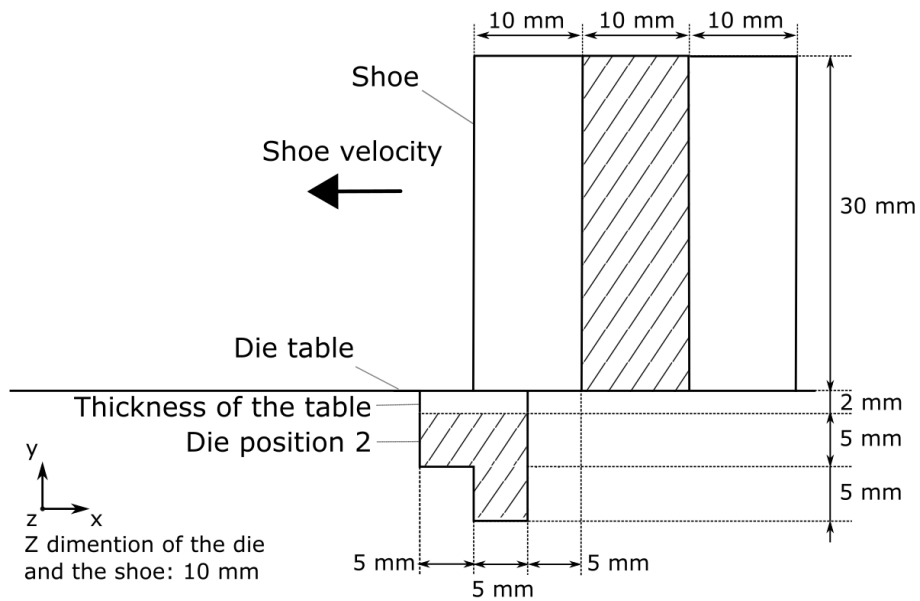Figure 3 - 2 Die filling system in the experiment

Figure 3 - 3 The die used in this validation test

(a) Regular, used in Case 1 and Case 2

(b) Rotated, used in Case 3 and Case 4

Figure 3 - 4 The schematic view of the die filling system in two positions

Table 3 - 1 Experimental conditions

Case	Shoe speed	Die position
Case 1-Exp	0.10 m/s	Position 1
Case 2-Exp	0.047 m/s	Position 1
Case 3-Exp	0.10 m/s	Position 2
Case 4-Exp	0.047 m/s	Position 2

3.2. Model description

The geometrical diagram of simulation of the die filling system according to the die position 1 are shown in Fig. 3-5. The geometry was created faithfully based on the dimensions of the experimental device. Cross-sectional slices of the fluid velocity field in x-y plane and y-z plane are expressed to show that how the air flow behave under a moving boundary system. Inside the die region, the air flow following the particle flow generated a vortex and remained as air cavities. The circulation of the air backflow escaped through the shoe's cavity. During this period, air flow acts against the down-coming particle flow in a relatively high magnitude (as the flow vector is colored in red). In the shoe cavity region, the overall flow vectors behaved the same as the shoe speed, stable and well aligned, noticing there is a small amount of air flowing outside the shoe's cavity at a relatively higher magnitude. This also implied that a certain amount of the air is leaking from the die to the outside environment. This phenomenon will be furtherly discussed in the following section. Table 3-2 shows the calculation conditions. In this study, two types of methods, single solid flow and gas-solid flow, were applied in order to investigate effect of air flow on particle

behavior. The numerical method for a single solid flow and a gas-solid flow is referred to as "Sim-S" and "Sim-GS", which represents that the DEM/SDF and the Advanced DEM-CFD method was utilized for single particle flows and gas-solid flows respectively. Each group had the same initial condition corresponding to the experiment test. As listed in the table, through Case 1 to Case 4, the shoe speed and die position are variables for the diversity of the comparison tests.

The physical properties of the particle and air are shown in Table 3-3. 150,000 particles were initiated for the tests whose initial positions were obtained by random packing and free falling. Particle size, density and Hamaker constant of the particle were assumed to be respectively 200 μm, 1,379 kg/m3 and 4.4×10-22 J corresponding to NONPAREIL-108® particle, which were also mentioned in the previous section. The cohesive force due to Van der Waals force is sufficiently smaller than gravitational force. In this study, there is hardly any particle agglomeration occurred and hence all the particle and the objective to be studied are spherical. We decided to use Ergun and Wen-Yu's equation. Spring constant, restitution coefficient and frictional coefficient were 50 N/m, 0.9 and 0.3, respectively. With the air condition being assumed, one can actually decide the Reynolds number roughly during the whole process. We have the shoe speed as fast as 0.1 m/s which gives us an order of -1. Let's take the order of the particle diameter, air density, air viscosity and we can estimate the Reynolds number is of the magnitude of 10^2, which is sufficiently less than 1000, referring to the Ergun

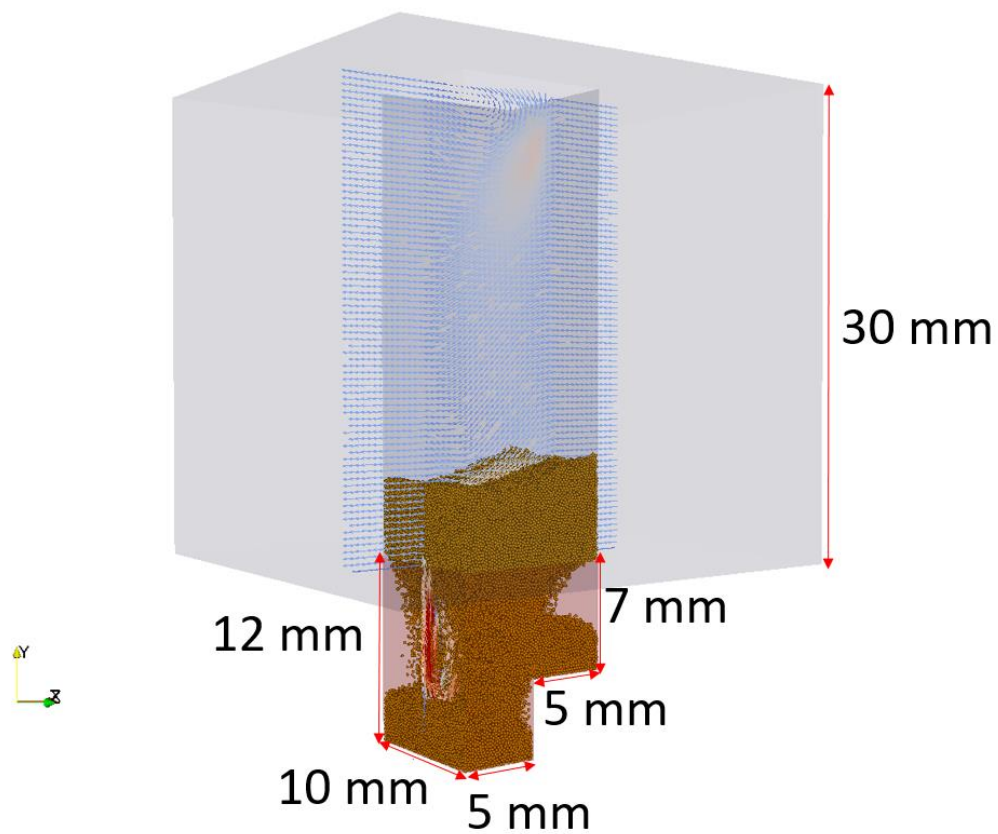and Wen-Yu's equation. Basically, the flow behavior of the air fluid can be considered as laminar flow.

Figure 3 - 5 3D geometry of the die filling system (Die: Position 1)

Table 3 - 2 Calculation conditions

Case	Phase	Shoe speed	Die position
Case 1-Sim-S	Solid	0.10 m/s	Position 1
Case 1-Sim-GS	Gas & Solid	0.10 m/s	Position 1
Case 2-Sim-S	Solid	0.047 m/s	Position 1
Case 2-Sim-GS	Gas & Solid	0.047 m/s	Position 1
Case 3-Sim-S	Solid	0.10 m/s	Position 2
Case 3-Sim-GS	Gas & Solid	0.10 m/s	Position 2
Case 4-Sim-S	Solid	0.047 m/s	Position 2
Case 4-Sim-GS	Gas & Solid	0.047 m/s	Position 2

Table 3 - 3 Physical properties of the solid and gas phase

Solid phase		
Particle number	-	150,000
Particle diameter	μm	200
Particle density	kg/m^3	1,379
Spring constant	N/m	50
Coefficient of restitution	-	0.9
Coefficient of friction	-	0.3
Hamaker constant	J	4.4×10^{-22}
Gas phase		
Air density	kg/m^3	1.0
Air viscosity	Pa·s	1.8×10^{-5}

3.3. Results and discussion

The experimental results will be firstly shown to demonstrate the differences between each cases with different calculation condition (shoe speed) and geometry setting (die position). Fig. 3-6 illustrates the snapshots obtained from experiments which are recorded by the high speed camera. The 4 cases were separated at the bottom of the figure where the detail

configuration of each case can be found in Table 3-2. The experiment for 0.10 m/s shoe speed, namely Case 1-Exp and 3-Exp, snapshots was obtained in 0.1 s, 0.125 s, 0.15 s and final state. In 0.047 m/s of shoe speed, namely Case 2-Exp and 4-Exp, snapshots was obtained in 0.15 s, 0.21 s, 0.26 s and final state. First, we may have a look on the influence brought by a change of the shoe speed.

In order to investigate effect of the shoe speed on powder injection in die position 1, we compared the results between Case 1-Exp and 2-Exp. The powder falling efficiency was influenced by the shoe velocity. As the shoe speed stayed normal, which is 0.1 m/s in Case 1, the fill ratio at the end of the process is not 1. An air cavity at the top-right could be observed in the die with a slope of the particle bed. However in Case 2, the die filling ratio was larger compared to the left column due to its slower shoe speed 0.047 m/s. In the final state, the die had been fully filled.

As far as the reversed direction of the die was concerned, tendency of the filling rate in position 2 was the same as that of the position 1. When the shoe speed was relatively-high such as in Case 3, the powder was not fully filled. When the shoe speed went lower, we can find that the die was fully filled. The geometry of the die also gave some influence at a certain magnitude. When we compare Case 1 and Case 3, as the first stage of the die (shallow part) close to the shoe's incoming direction, the particle flow firstly hit the solid structure at T = 0.1 s in Case 1. As in Case 3, the deep die stage is closer to the shoe's incoming direction, the particle flow were still falling to the

bottom of the die. Consequently, the powder filling rate was shown to be influenced by shoe speed and the die geometries according to the experimental results.

In Fig. 3-7, the simulation results using the DEM/SDF and the Advanced DEM-CFD method were shown alongside with the Experimental data. The snapshots were taken at the same time point during the process. As the first column has been shown previously, let us have a direct look at the second column, where the DEM/SDF simulation results were indicated. It is indicated as Sim-S, standing for the simulation with single phase flow (particulate flow). In the early phase of the die filling process, there was not a clear difference compared to the experiment. However after T = 0.15 s, where the appearance between the two results were totally different. In the experiment, there were still three large cavities located in the top-right, bottom-right and the left part. However in the Sim-S result, it showed a nearly fully filled die with just a small size air cavity located at the top-right part of the die. At the final state, we can observe that the die is fully filled at Sim-S compared to the experiment, which could be a complete misleading when doing simulations for the actual die filling process. The numerical method for DEM/SDF is not sufficient to cover all cases of the die filling systems and therefore we applied the Advanced DEM-CFD method in the third column. It is noted as Sim-GS, which stands for the simulation in both gas and solid phase, namely, the air fluid and the particles. In this approach, as we can clearly observe in the comparison figure, the appearance from the

simulation results got much more improved. Although this phenomenon may not be vividly illustrated at T = 0.1 s, where it was the very early state of the filling process. The following figures gave a more and more clear differences compared to the Sim-S, especially at T = 0.15 s where a clear difference was also shown between the experiment and the Sim-S. In Sim-GS, the main air cavities were successfully predicted compared to the real case in the experiment. The amount of particles fell into the die is larger in a qualitative point of view. As in the final state demonstrated, there was a slope remaining at the top of the particle bed, which was identical to the slope in the final state of the experiment.

In Fig. 3-8, the snapshot comparison was shown for the Case 2, where the shoe speed dropped down to 0.047 m/s, as almost half as it was in Case 1. It has been noticed that when the particle flow touched down on the surface of the shallow stage in the die, the position is just almost half way compared to the Case 1, which is also an interesting effect brought by a change of speed. The situation was the same as it was in the Case 1, there was hardly any vivid differences among the experiment, Sim-S and Sim-GS results in the early phase of this process. After T = 0.26 s, it can be found that the Sim-S result already showed a fully filled die, despite of a small cavity at the surface of the particle bed, which is inside the table's thickness area. This is a prediction failure of the actual case in the experiment, as one can observe in the first column. However the Sim-GS result predicted a better appearance for this situation. The three cavities can be observed in the corresponding positions

towards the experiment in a good agreement. At the final state, since the shoe speed had been decreased by more than half of its original speed, all the dies were fully filled as we expected.

Fig. 3-9 shows a snapshot comparison for Case 3. In Case 3, the die's position has been reversed by 180 degree compared to Case 1. Now the shallow stage of the die located at the opposite direction and the deeper stage came closer to the shoe's incoming direction. As the shoe speed stayed as 0.1 m/s, the final die filling ratio was not dramatically changed compared to Case 1. However it can still demonstrate the influence brought by air interaction with particles once it is considered. To have a closer look at the die part, again we only focused at the later phase. As an example, at T = 0.15 s, we have a similar appearance occurred in both experiment and the Sim-GS results, the size and the location of the cavities were all predicted correctly in calculation. However in the Sim-S results, the appearance showed a nearly fully filled die with a small air cavity located at the top-right part of the die. This inconsistency also demonstrated that the single phase simulation is not capable of calculating all the die filling systems. As the final state results showed, in the experiment, we have a partially filled die with a slope at the top of the particle bed. Yet the Sim-S calculation returned a fully filled die. However Sim-GS calculation showed also a partially filled die with a similar slope located at the top of the particle bed just as it is shown in the experiment.

With the Fig. 3-10 showing Case 4 results, the status also showed that the Sim-S calculation could not fully reproduce the die filling process under some certain conditions. In Case 4, the position of the die had been reversed compared to Case 1, and the shoe speed was slowed down to 0.047 m/s as the same as Case 3. In this particular case, the difference of the results even appeared at an early stage at T = 0.21 s. At this time, one may clearly observe the experimental snapshot, the particle flow had just reached the shallow stage of the die at the left part, which was similarly reproduced in the Sim-GS results in the third column. However in the Sim-S calculation, the particle flow had already reached at the left part stage with an amount of particles laying on the surface. In the next row, the comparison showed a main difference just as the previous cases. During the later phase of the filling process, the experiment results filling rate is obviously lower than that of the Sim-S calculation. The left and right part of the die still remained large air cavities, which were successfully predicted in Sim-GS case. As a final state, all the dies were fully filled due to a sufficient lower shoe speed.
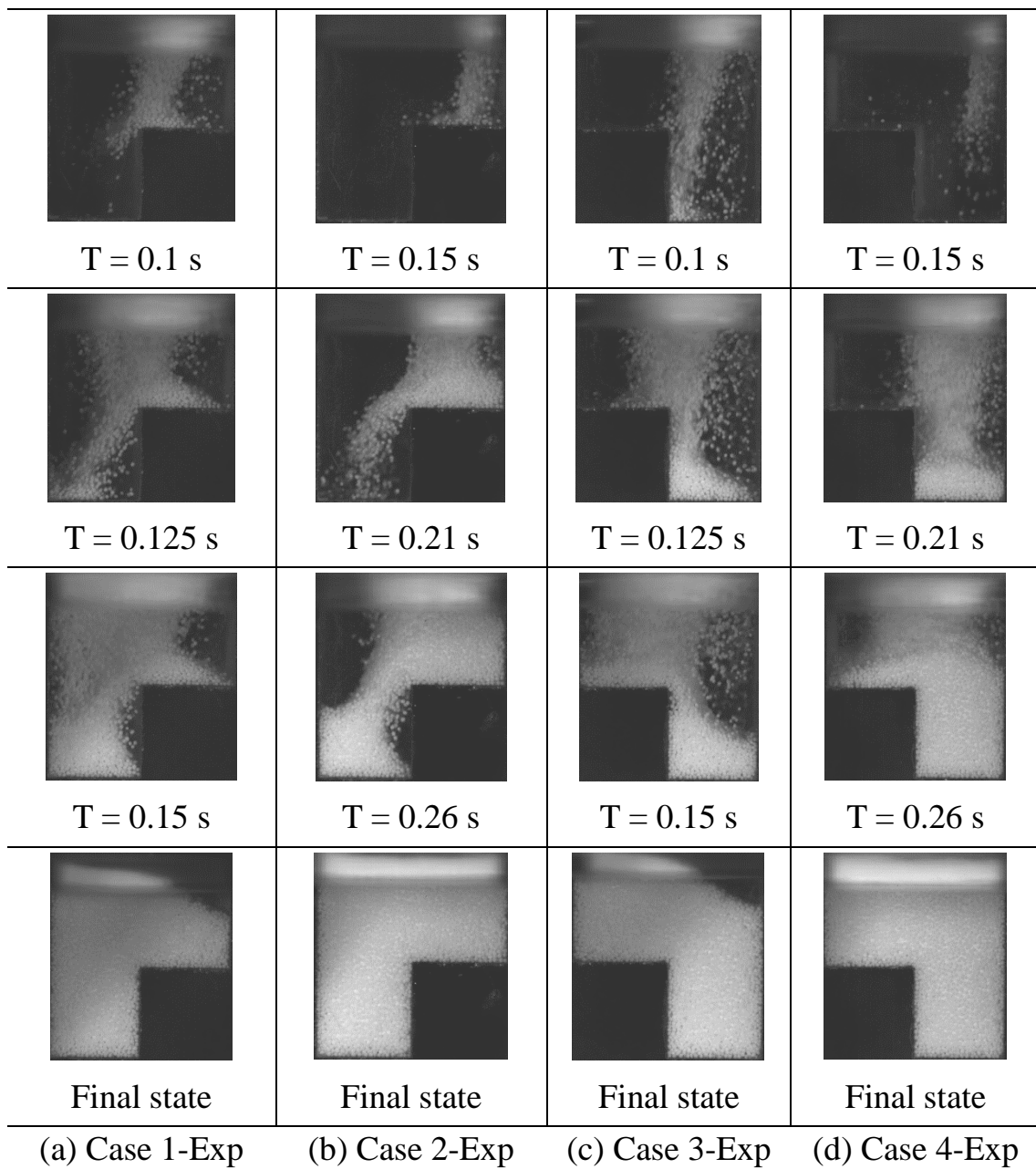
T = 0.1 s	T = 0.15 s	T = 0.1 s	T = 0.15 s
T = 0.125 s	T = 0.21 s	T = 0.125 s	T = 0.21 s
T = 0.15 s	T = 0.26 s	T = 0.15 s	T = 0.26 s
Final state	Final state	Final state	Final state
(a) Case 1-Exp	(b) Case 2-Exp	(c) Case 3-Exp	(d) Case 4-Exp

Figure 3 - 6 Snapshots comparison between experimental results under different conditions

53

T = 0.1 s	T = 0.1 s	T = 0.1 s
T = 0.125 s	T = 0.125 s	T = 0.125 s
T = 0.15 s	T = 0.15 s	T = 0.15 s
Final state Exp	Final state Sim-S	Final state Sim-GS
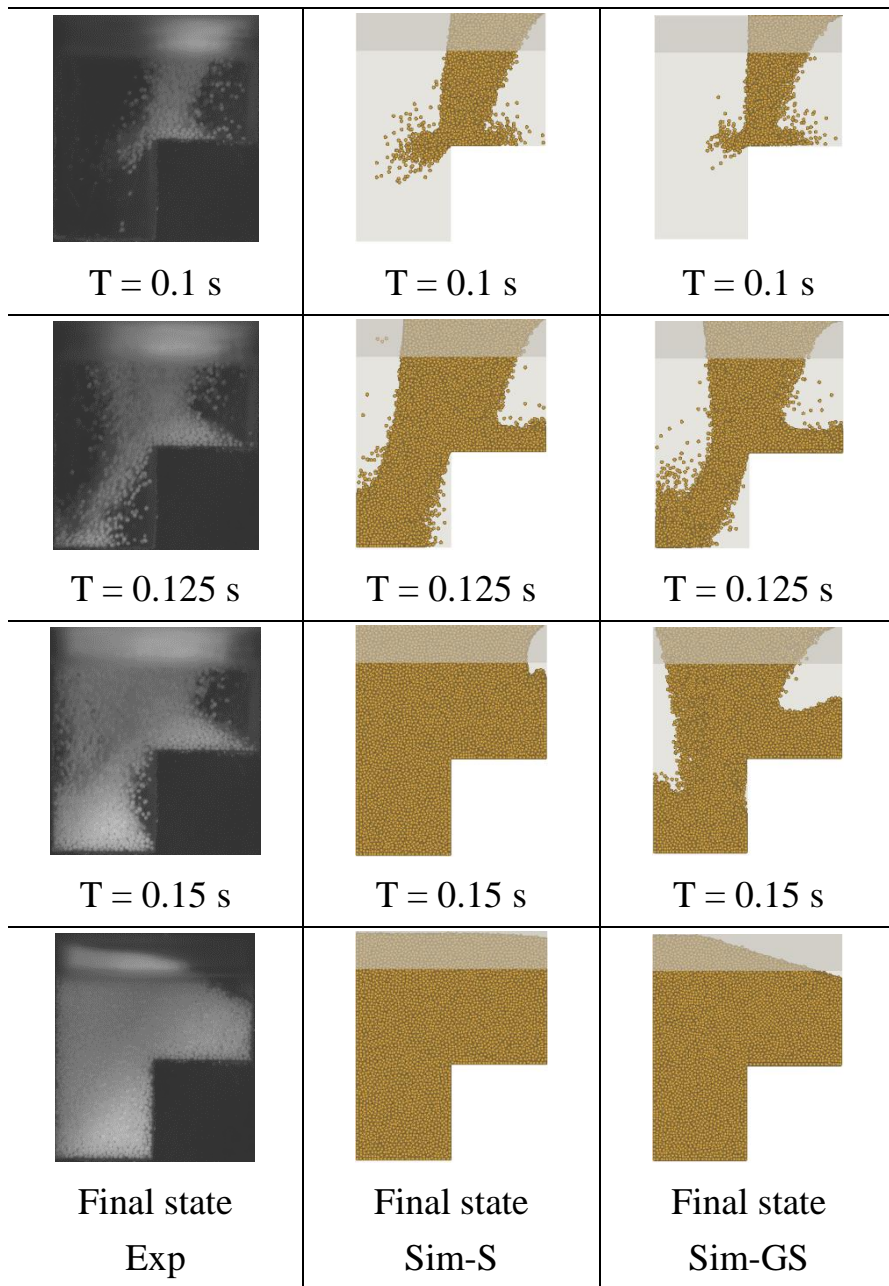
Figure 3 - 7 Case 1 comparison

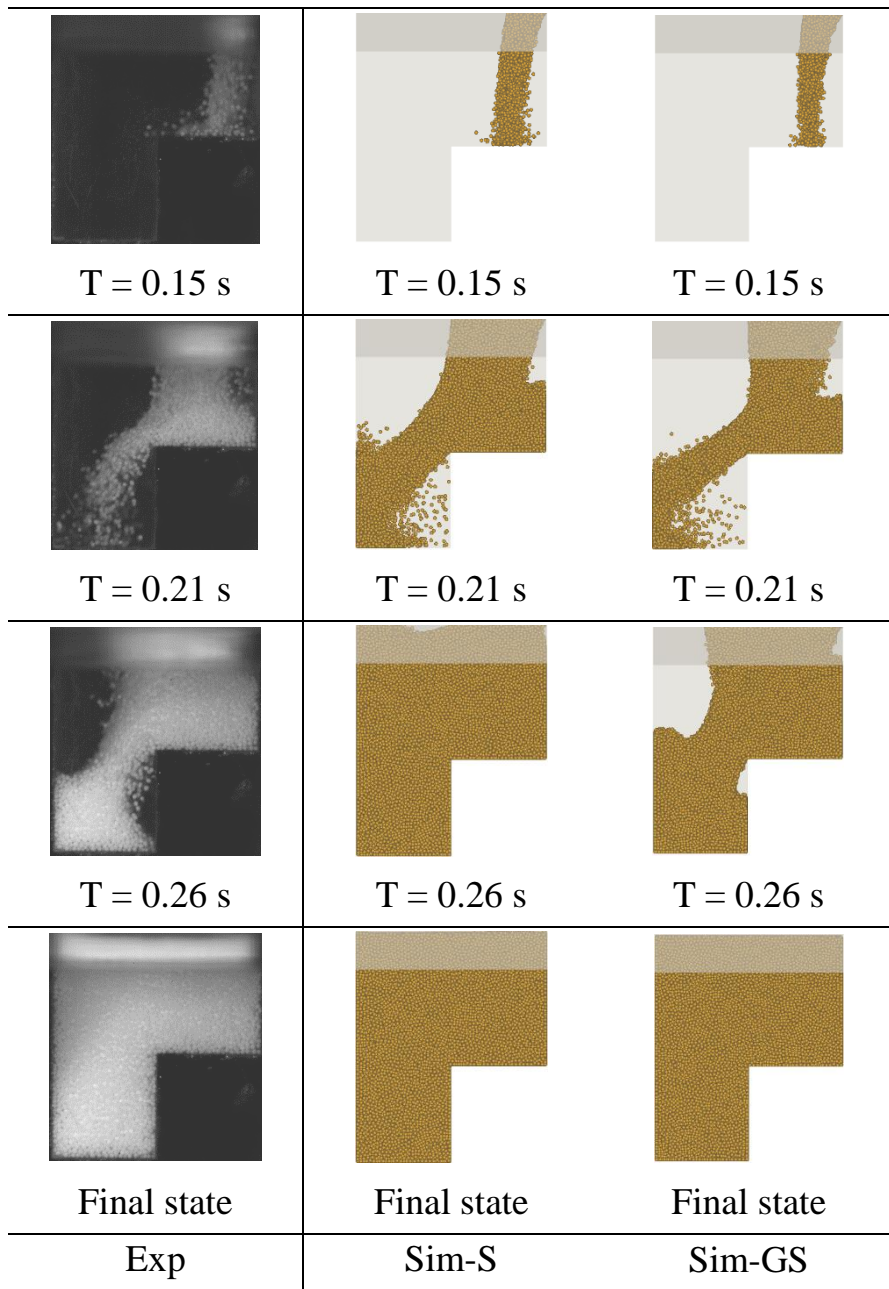| T = 0.15 s | T = 0.15 s | T = 0.15 s |
T = 0.21 s	T = 0.21 s	T = 0.21 s
T = 0.26 s	T = 0.26 s	T = 0.26 s
Final state	Final state	Final state
Exp	Sim-S	Sim-GS

Figure 3 - 8 Case 2 comparison
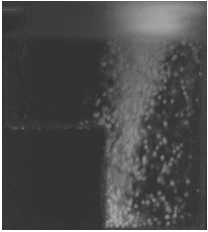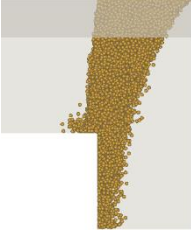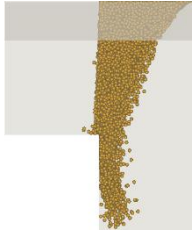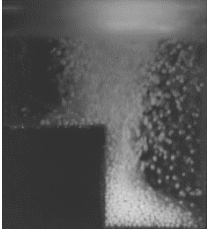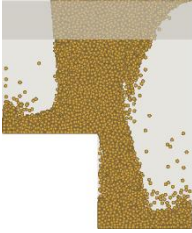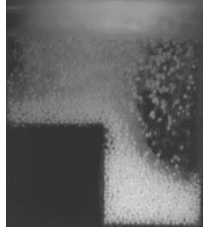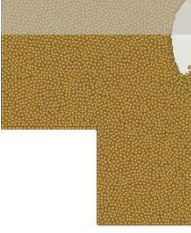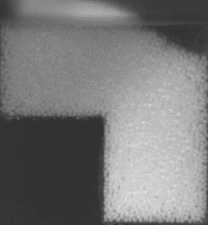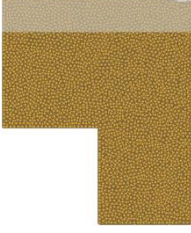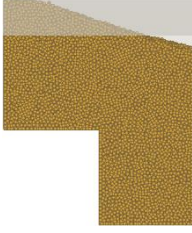
T = 0.1 s	T = 0.1 s	T = 0.1 s
T = 0.125 s	T = 0.125 s	T = 0.125 s
T = 0.15 s	T = 0.15 s	T = 0.15 s
Final state	Final state	Final state
Exp	Sim-S	Sim-GS

Figure 3 - 9 Case 3 comparison

T = 0.15 s	T = 0.15 s	T = 0.15 s
T = 0.21 s	T = 0.21 s	T = 0.21 s
T = 0.26 s	T = 0.26 s	T = 0.26 s
Final state	Final state	Final state
Exp	Sim-S	Sim-GS

Figure 3 - 10 Case 4 comparison

When the air fluid is considered in the Sim-GS, the calculation results became much improved over all the cases in this study. This is because the interaction between air and particle became dominant in this die filling

system. The drag force can results in a strong force that influences the particle flow movement. The study regarding how the air flow will have an influence on the particle flow was discussed experimentally by Wu's team. In their case, the size of the particle used in their experiment was so small that the influence brought by the ai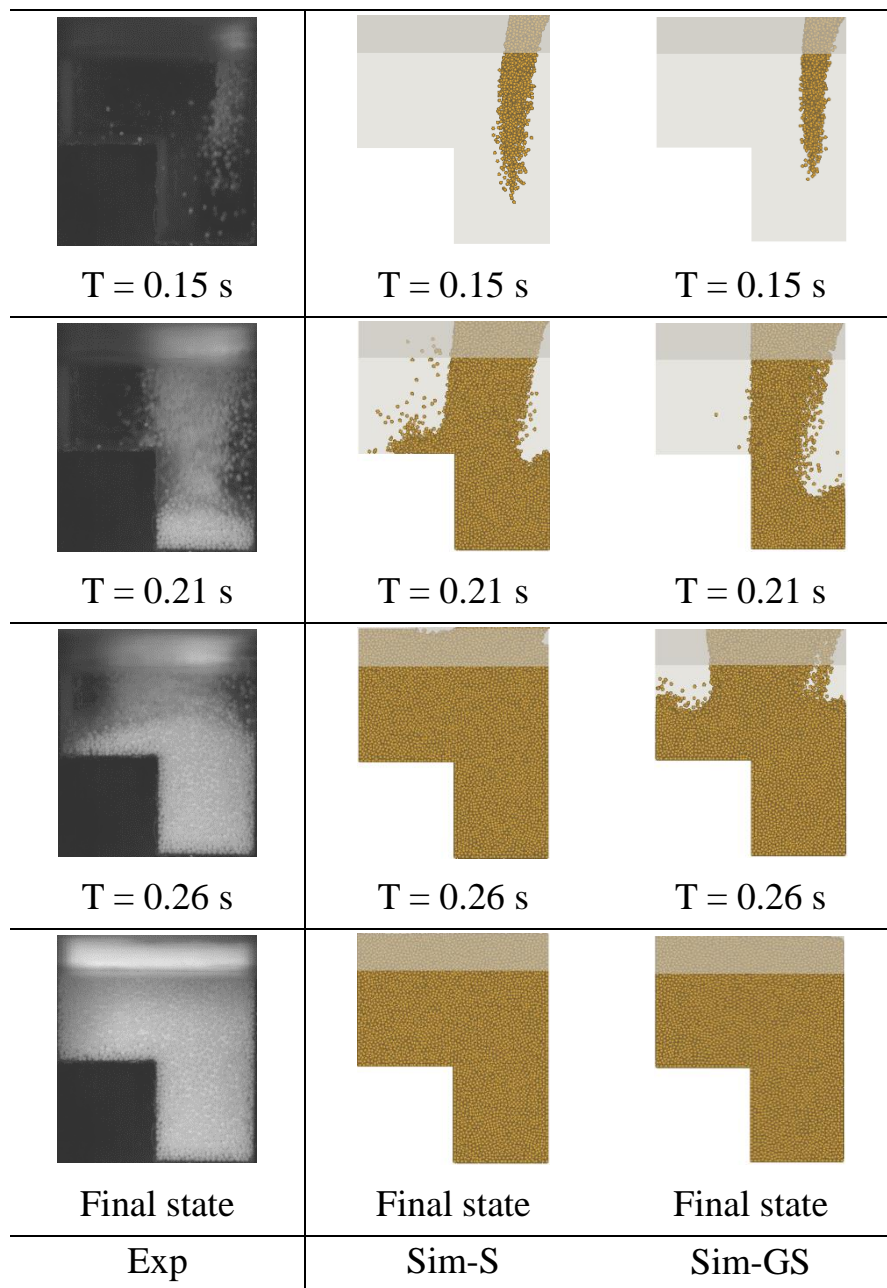r could be large enough to be considerable. In previous DEM simulation studies for die filling system, the particles concerned in their researches were at a relatively large size so that the air flow could bring less influence on each single particle, in which case the interaction between air and solid particle may be neglected. Besides, the results using only DEM equations to govern those problems turned out to be sufficient enough in the validation tests. Therefore, as previous study have proven, as long as the granule diameter is large enough to be larger than 500 micrometers, the results for a single phase calculation could be acceptable.

In the current case however, the particle size of the die filling system have become 200 micrometer diameter as the shown in Table 3-3. The effect from air flow will be stronger for fine particle systems, in which case the interaction could not be neglected. As in DEM/SDF method, the calculation results failed to reproduce the whole die filling procedure by over-predicting more particles deposited inside the die. After the Advanced DEM-CFD method has been introduced, we can find that the air acting as a continuum fluid plays such an important role during the whole process. More than that, the application of the Immersed Boundary Method makes it possible to model actual die filling system in the industry by considering a moving

boundary. Since the movement of the boundary can literally interact with the air fluid, the modeled processes were able to be much more real to the industry point of view.

In order to have a closer look at the behavior of the air, Fig. 3-11 shows the volume fraction expression for all 4 cases of the Sim-GS with the visualized air vectors. Case 1 to Case 4 were listed in the 1 to 4 columns. As an example of explanation, we firstly pick Case 1 to demonstrate this effect. As the scale showed, white part represents epsilon around 0.4, namely the particle phase being dominant. At $T = 0.1$ s, the air fluid already formulated a vortex at the top-right part of the die. This is because the shoe structure had already come to cover the top of the die, which blocked the deposition area of the table and make the inner die space a closed environment. Thus when the particle flow initially dropped down, the air followed the nose flow until touched on the shallow stage thus reflected back. The backflow from the air separated into two main directions, forward as the shoe's movement direction and backwards, along which the air furtherly hit on the right wall and then flew upwards. Due to the geometry of the die, an air circulation was created. When air was flowing upwards, it contradicted the particle flow, which was flowing down, and moderated the particle's free falling phenomenon. At $T = 0.125$ s, the air's movement was getting intense. There were totally three main blocks of air that separated the die's inner space. The speed of the air flow was also increased as one can see from the color range indicator. The highest velocity shoot up to 0.4 m/s at the branches of the

backflow located at the bottom surface. At T = 0.15 s, the three blocks separated by particle flow developed into smaller air cavities. We have noticed that these three cavities were predicted nicely compared to the experiment. At the final state, all movement were settled down therefore no air vector can be seen and resulted in a partially filled die. In Case 2, since the shoe speed was decreased by half, the total energy of the whole system was also expected to be lower. By observing the air vector, the magnitude of the air velocity during the whole process was lower than Case 1 at every time points respectively, given that the red-colored arrows and the length of the visualized vectors were degraded compared to the Case 1. Despite of a reversed die geometry, the same fashion was demonstrated in Case 3 and Case 4.

The qualitative comparison results showed a good agreement for the Advanced DEM-CFD validation test, meanwhile it has been proven that only with the Advanced DEM-CFD method can a fine particle die filling system been well predicted. Now let us turn to a quantitative comparison for the edge point distance. The edge point distance is a common feature to assess the similarity from validation tests in die filling process. Due to the difficulty of access all kinds of data from the experiment, we rely on the most accurate measurement that is by using the high speed camera. The other properties like pressure, or mass comparison will be introduced in the verification study. The measuring way is illustrated in Fig. 3-12, the distance is measured between the right inner surface and the edge of other side of the particle flow.

The height of the origin point corresponds to the half height of the particle flow. All the comparison data was shown in Fig. 3-13. In each case, the edge point distance was compared between experimental data and Sim-GS calculation data. From the figure one may conclude that the calculated results were consistent with the experimental data, given most of the data points were coincident with each other. In Fig. 3-14, the unfilled area was marked by the red triangle at the end of the process. The empty area ratio (S_{empty}/S_{total}) percentage was calculated in Case 1 and Case 3, given the fact that only these two cases with lower shoe speeds are partially filled. Both of the cases the error appeared to be less than 5%. Qualitatively, the behavior from actual die filling experiments was captured by using the Advanced DEM-CFD method.

T = 0.1 s	T = 0.15 s	T = 0.1 s	T = 0.15 s
T = 0.125 s	T = 0.21 s	T = 0.125 s	T = 0.21 s
T = 0.15 s	T = 0.26 s	T = 0.15 s	T = 0.26 s
Final state	Final state	Final state	Final state

Scale

(a) Case 1-Sim-GS	(b) Case 2-Sim-GS	(c) Case 3-Sim-GS	(d) Case 4-Sim-GS
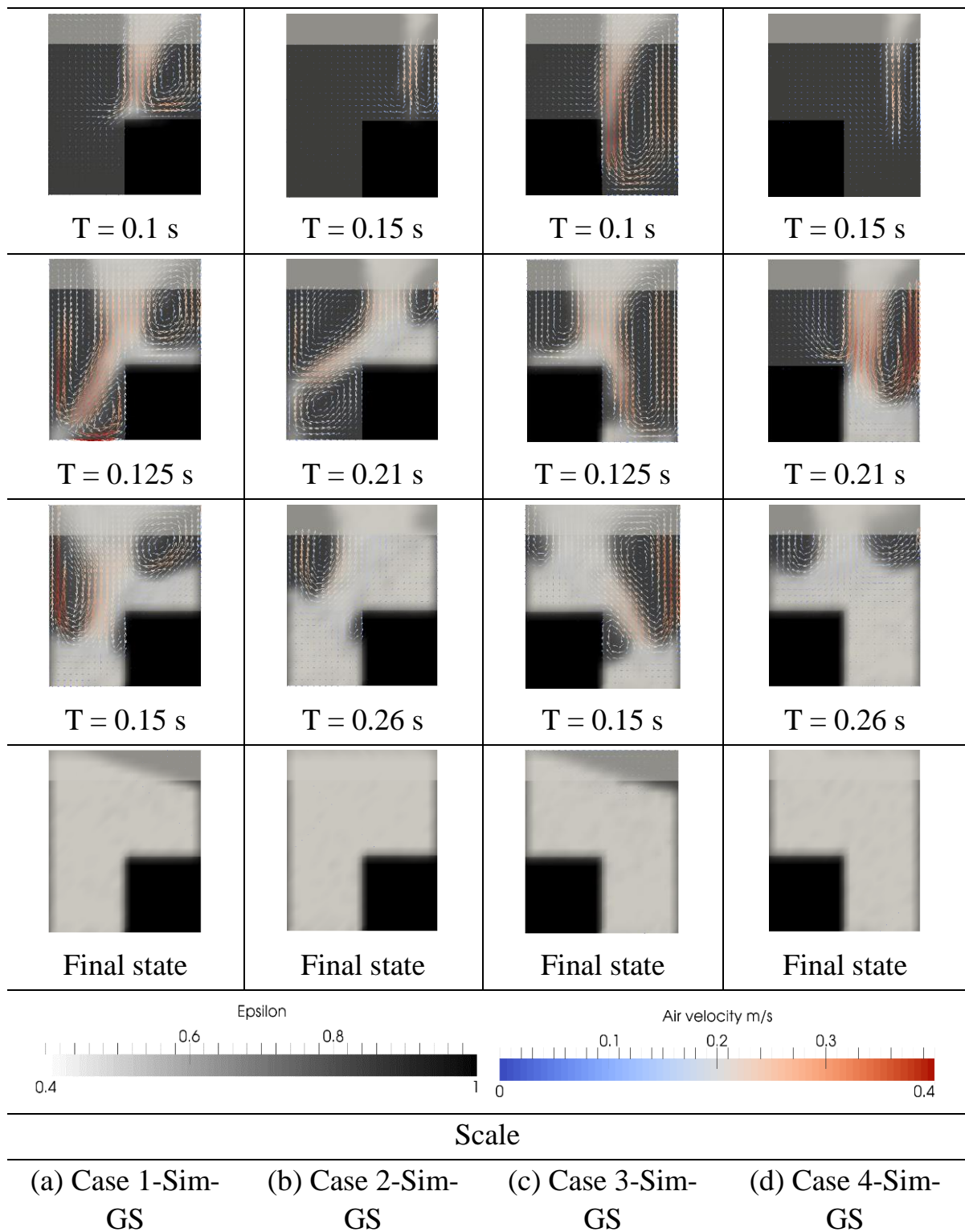
Figure 3 - 11 Volume fraction of solid phase and air flow vector obtained from the Advanced DEM-CFD method
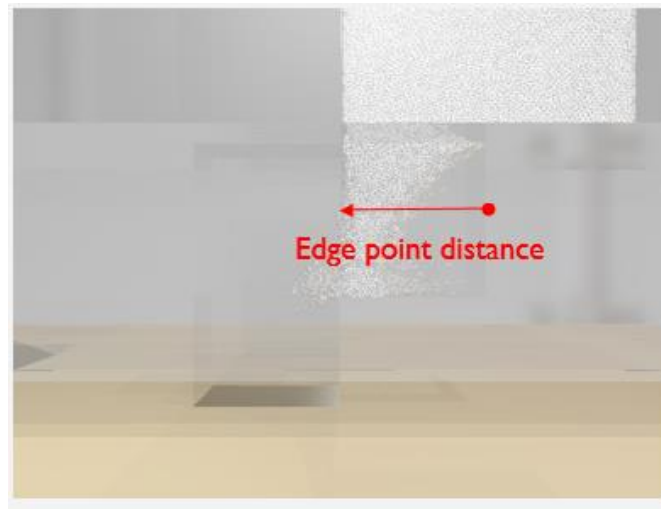
Figure 3 - 12 An illustration of edge point distance

(a) Case 1   (b) Case 2

(c) Case 3   (d) Case 4
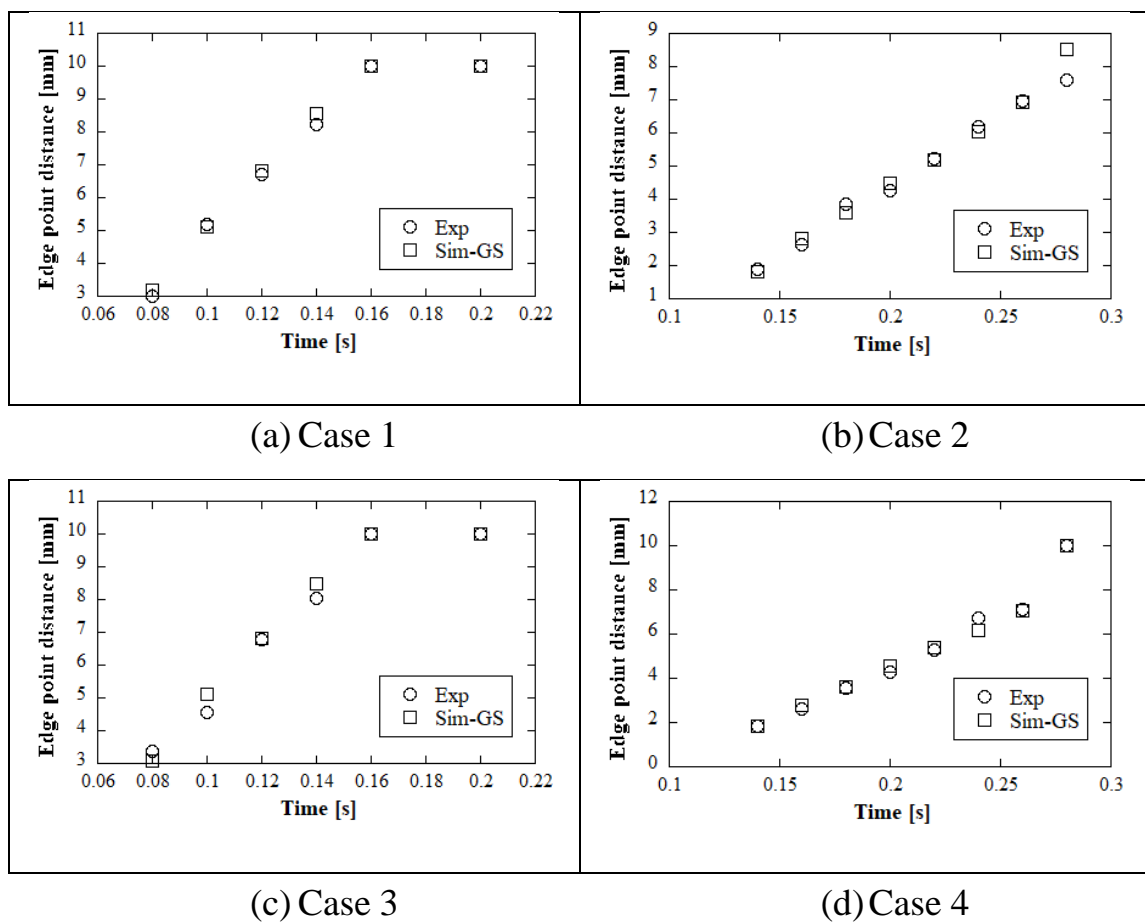
Figure 3 - 13 Edge point distance comparison between experiment and the Advanced DEM-CFD method in 4 cases.
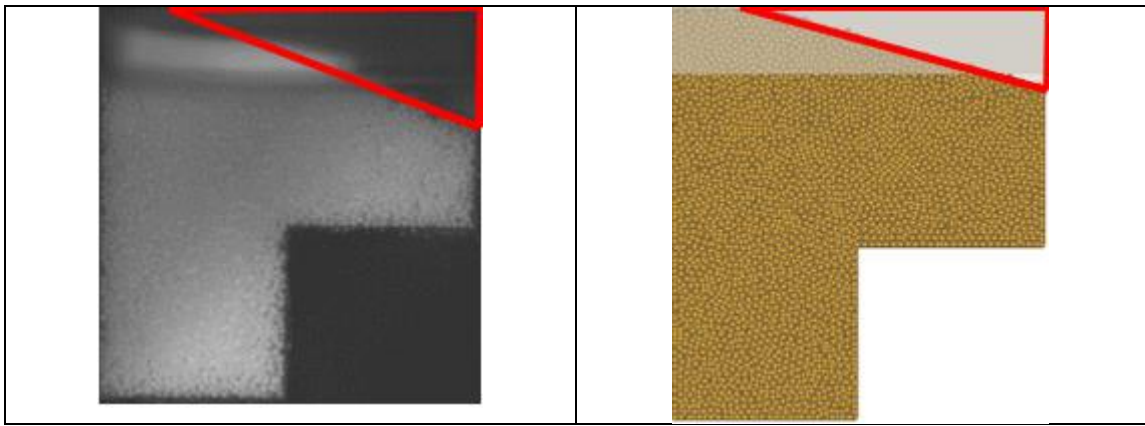
| 11.38% | 9.71% |

(a). Case 1
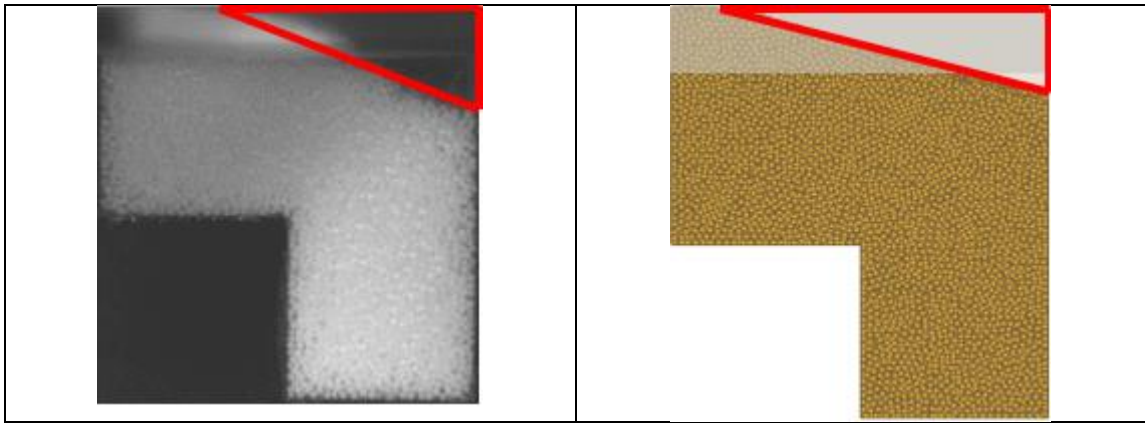
| 10.79% | (a) 12.28% |

(b). Case 3

Figure 3 - 14 Empty area ratio percentage comparison at the final states

Chapter 4   Conclusions

As a closing chapter for this doctoral dissertation, a summary of the works done will be systematically organized. In the first section of this chapter, objective and achieved results will be again emphasized, which is the main idea of this study. Next section will make a summary through Chapter 3 to Chapter 5, talk about the achievement in a global perspective. In the final section, works that still remained or could be done in the future will be mentioned. And a few viewpoint of the die filling process in the industry as well as the numerical simulation will also be shortly discussed.

4.1.   Objectives and achieved results

Through this doctoral project, the numerical modeling for the industrial die filling system is discussed. Background of the die filling system and the development of its modeling have been introduced in the first chapter. Among all of those existing numerical approach, several problems and difficulties remained for this particularly process. The special treatment of a moving boundary which involves the combination between SDF and IBM has helped us successfully predicting the actual die filling system. To restate the objectives of this study, these problems and difficulties that we have overcome are listed in following:

- 2D system is easily to be constructed however, complicated 3D modeling

is not frequently applied.

The progression of numerical methods is becoming faster and faster, meaning a 3D system would not be a general problem in most of the approaches, to build a 3D system by using signed distance function that generates Lagrangian pixels at ease is an elegant fashion for building complicated geometry, as long as the CAD is triangulated. Given the fact that a traditional mesh model is algorithmically complicated to build, only simple geometries were tested in the past studies. Utilizing signed distance function based boundary, the geometry can be created with all kinds of shapes and dimensions.

- None modeling are available in the mesh-based model. The interaction between moving wall and air is ignored, i.e., a real wall boundary is improbable to model.

The simple and efficient combination between signed distance function and immersed boundary method provides a great approach at this circumstance. In the IBM, the volume fraction parameter is acquired from the SDF-based grids. By doing so, the movement of the boundary can be modeled in the local averaged Navier-Stokes equations and thus influence the velocity field in Eulerian mesh, i.e., the continuous fluid velocity. In die filling system, this method is extremely important since the delivery of particle itself is a crucial process during the whole process. Only by using this method, can we successfully model a moving boundary with wall thickness considered, and influencing the particle phase and air phase.

● A large-scale approach for industrial die filling process.

In the introduction chapter, a large scaling method called EMMS for fluidized bed is mentioned and discussed. Basically this method is dedicated for the dense phase during the fluidization. The kinetic energy conservation model is designed for a regular shaped cluster geometry, a large sphere. In die filling system, the appearance of the particle flow is highly depended on the geometry condition and hardly spherical. Thus we proposed the coarse grain model for DEM particles and applied this modeling onto the Advanced DEM-CFD method. The settings and results were introduced in Chapter 4 and Chapter 5. Its applicability is very promising throughout these tests.

4.2. Summary of works

The research results of this doctoral project have been demonstrated in Chapter 3 – 5. In Chapter 3, validation tests were performed for the firstly proposed Advanced DEM-CFD method. We tested our method under the die filling system with two different shoe speeds and two different geometry setups. With these different calculation conditions being built, both the newly developed Advanced DEM-CFD method and the previously used DEM/SDF method were applied to test the difference and improvement of the results. By comparing both calculated results with the experimental data, it is proven that the Advanced DEM-CFD method is generally applicable for

die filling systems especially when the size of the particle is small. In that situation, a DEM/SDF method is not capable of reproducing the actual process since the fine particle is effected by the air flow much easier than a large particle case. The main comparison data is the qualitative appearance of the front view of the die at several time point during the filling process. A quantitative comparison was also added for the edge point distance of the particle flow. Consequently speaking, the adequacy of the Advanced DEM-CFD method is proven.

In Chapter 4, a coarse grain model is applied on the Advanced DEM-CFD method to scale-up the die filling system. In this chapter, two groups of tests were introduced as a first step for the large scale modeling. The geometry was constructed with simple geometry and the coarse graining particle size was set to be doubled and tripled to the original particle size, which is 100 micrometer. More than that, a simply large case was also conducted as the comparison test. The results were as expected. The comparison data showed that with the coarse grain model employed, the coarse grain ratio results were in good agreement with each other. This is because the kinetic energy is conserved by modeling the DEM particle forces. As a side prove, the simply large case results were totally different despite of having the same particle size. However the geometry was quite simple and thus cannot fully prove the adequacy of the method. We wanted to test this approach with its full capacity, thus the next chapter was added.

Chapter 5 is also a verification study regarding the large scaling problem, or to say a further study based on Chapter 4. In this chapter, an obstacle is equipped inside the die to raise the complexity of the geometry. The results showed that once the geometry become too narrow, the coarse graining particle could behave differently compared with the original particle. This phenomenon is reflected through the appearance of the final state particle bed, where the angle of repose in the original case is clearly much smaller than that of a high CGR case. The reason that caused this inconsistency is most likely because that the size of the DEM particle is too large to be in a CFD gird. Since the local averaged technique is depended on the number of particles inside one gird, with a large size of the particle, there would not be sufficient number of particle and the error of the modeling will increase. To prove that, in the second group, the particle size has shrunk 20%. With the geometrical data and other particle properties unchanged, the new CGR tests showed a much better agreement as the angle of repose at the final state had less error in the CGR cases.

4.3. Future development

Various tests have been conducted including experiment to help us understand the characteristics of a die filling system. We have accomplished a large amount of data and results by applying the Advanced DEM-CFD method. Nevertheless, there are still some topics and fields remained in die filling process that are interesting and promising to dig in.

- Lid effect

In a typical die filling system, the shoe which delivers the packed fine particles could usually be moving with a lid on its top. A lid functions like a cap that covers the top of the cavity so that the shoe's cavity will no longer be in contact or exchange substance with the outside atmosphere, as many processes would behave like this. The idea of a lid covering on the shoe is to make sure that during a fully packed shoe's movement, no particles can leak outside such that the whole table will be in a mess with fine particles or more seriously, it is a waste of raw material and could cause other part of the mechanism operated wrongly. A simulation that considers lid effect is realistic and a good path to test the ability of numerical codes.

- Particle segregation

Particle segregation is actually one of the most popular topic existed in particulate flow studies. This phenomenon is involved in many fields of chemical engineering. To study on segregation means to initiate at least two kinds of particles with different sizes and check the distribution inside the die and overall behavior during the filling process.

- Continuous filling process

As mentioned in the introduction part, some of the die filling process was not only involved with one die under the table. A continuous filling means

that a table that rotates along the central axis and at its periphery several deposition areas with dies beneath the table are located. In this system, the shoe moves circularly instead of linear. And since there are multiple dies existing, the total number of particle and physical time are expected to be a lot more than a single filling case.

The aforementioned three items are the topics that author believe to have great potential and significance on numerical modeling. Each topic has its unique identity and characteristic. Either it is more concentrated on detailed flow movement, or the interphase interactions, or even a macroscopic viewpoint of the process. Experimental research on the other hand, has its own difficulty since every time the particle should be cleaned within the system and visualization or the measurement is hard to perform. Despite all this, experimental data is valuable and instructive for code developing and sensitive analysis. Different types of particles could also be used such as iron powder. There is still many uncovered territories in this field and the author wish those unknown will be discovered and understood in the near future.

References

[1]   L. A. Mills and I. C. Sinka, "Effect of particle size and density on the die fill of powders," *Eur. J. Pharm. Biopharm.*, vol. 84, no. 3, pp. 642–652, Aug. 2013.

[2]   AZO MATERIALS, "Understanding Die Filling Behavior in Powder Metallurgy Printable Document." [Online]. Available: https://www.azom.com/article.aspx?ArticleID=4863#. [Accessed: 12-Nov-2018].

[3]   J. H. Jeong and D. Y. Yang, "Application of an adaptive grid refinement technique to three-dimensional finite element analysis of the filling stage in the die-casting process," *J. Mater. Process. Technol.*, vol. 111, no. 1–3, pp. 59–63, Apr. 2001.

[4]   C. Giardini, E. Ceretti, and G. Maccarini, "Formability in extrusion forging: The influence of die geometry and friction conditions," *J. Mater. Process. Technol.*, vol. 54, no. 1–4, pp. 302–308, Oct. 1995.

[5]   L. C. R. Schneider, I. C. Sinka, and A. C. F. Cocks, "Characterisation of the flow behaviour of pharmaceutical powders using a model die-shoe filling system," *Powder Technol.*, vol. 173, no. 1, pp. 59–71, 2007.

[6]   D. Mateo-ortiz and R. Méndez, "Relationship between residence time distribution and forces applied by paddles on powder attrition during the die filling process," *Powder Technol.*, vol. 278, pp. 111–117, 2015.

[7]   M. Elyasi, M. Bakhshi-Jooybari, and A. Gorji, "Mechanism of improvement of die corner filling in a new hydroforming die for stepped tubes," *Mater. Des.*, vol. 30, no. 9, pp. 3824–3830, Oct. 2009.

[8]   D. Aole, M. K. Jain, and M. Bruhis, "New characterization methods for powder die fill process for producing powder metallurgical components," *Powder Technol.*, vol. 232, pp. 7–17, Dec. 2012.

[9]   E. N. Nwose and C. Pei, "Modelling die filling with charged particles using DEM/CFD," *Particuology*, vol. 10, no. 2, pp. 229–235, Apr. 2012.

[10]   I. C. Sinka, L. C. R. Schneider, and A. C. F. Cocks, "Measurement of the flow properties of powders with special reference to die fill," *Int. J. Pharm.*, vol. 280, no. 1–2, pp. 27–38, Aug. 2004.

[11] C.-Y. Wu, B. Armstrong, and N. Vlachos, "Characterization of Powder Flowability for Die Filling," *Part. Sci. Technol.*, vol. 30, no. 4, pp. 378–389, Jul. 2012.

[12] M. Gentzler, J. N. Michaels, and G. I. Tardos, "Quantification of segregation potential for polydisperse , cohesive , multi-component powders and prediction of tablet die-filling performance – A methodology for practical testing , re-formulation and process design," *Powder Technol.*, vol. 285, pp. 96–102, 2015.

[13] D. Mateo-ortiz, F. J. Muzzio, and R. Méndez, "Particle size segregation promoted by powder fl ow in con fi ned space : The die fi lling process case," vol. 262, pp. 215–222, 2014.

[14] Y. Guo, C. Wu, and C. Thornton, "The effects of air and particle density difference on segregation of powder mixtures during die filling," vol. 66, pp. 661–673, 2011.

[15] D. Di Carlo, J. F. Edd, K. J. Humphry, H. A. Stone, and M. Toner, "Particle segregation and dynamics in confined flows," *Phys. Rev. Lett.*, vol. 102, no. 9, pp. 1–4, 2009.

[16] Y. Guo, C. Y. Wu, K. D. Kafui, and C. Thornton, "Numerical analysis of density-induced segregation during die filling," *Powder Technol.*, vol. 197, no. 1–2, pp. 111–119, Jan. 2010.

[17] R. Maione, S. Kiesgen De Richter, G. Mauviel, and G. Wild, "Axial segregation of a binary mixture in a rotating tumbler with non-spherical particles: Experiments and DEM model validation," *Powder Technol.*, vol. 306, pp. 120–129, 2017.

[18] Y. Guo, C. Wu, K. D. Kafui, and C. Thornton, "Numerical analysis of density-induced segregation during die filling," *Powder Technol.*, vol. 197, no. 1–2, pp. 111–119, 2009.

[19] C. Ramírez-Aragón, F. Alba-Elías, A. González-Marcos, and J. Ordieres-Meré, "Segregation in the tank of a rotary tablet press machine using experimental and discrete element methods," *Powder Technol.*, vol. 328, pp. 452–469, Apr. 2018.

[20] C. Hildebrandt, S. R. Gopireddy, R. Scherließ, and N. A. Urbanetz, "Simulation of particle size segregation in a pharmaceutical tablet press lab-scale gravity feeder," *Adv. Powder Technol.*, vol. 29, no. 3, pp. 765–780, Mar. 2018.

[21]   S. Jackson, I. C. Sinka, and A. C. F. Cocks, "The effect of suction during die fill on a rotary tablet press," *Eur. J. Pharm. Biopharm.*, vol. 65, no. 2, pp. 253–256, Feb. 2007.

[22]   A. Zakhvatayeva, W. Zhong, H. A. Makroo, C. Hare, and C. Y. Wu, "An experimental study of die filling of pharmaceutical powders using a rotary die filling system," *Int. J. Pharm.*, vol. 553, no. 1–2, pp. 84–96, Dec. 2018.

[23]   H. P. Goh, P. W. S. Heng, and C. V. Liew, "Understanding die fill variation during mini-tablet production," *Int. J. Pharm.*, vol. 534, no. 1–2, pp. 279–286, Dec. 2017.

[24]   W. Grymonpré *et al.*, "In-line monitoring of compaction properties on a rotary tablet press during tablet manufacturing of hot-melt extruded amorphous solid dispersions," *Int. J. Pharm.*, vol. 517, no. 1–2, pp. 348–358, Jan. 2017.

[25]   N. Tarlier *et al.*, "Deformation behavior of crystallized mannitol during compression using a rotary tablet press simulator," *Int. J. Pharm.*, vol. 547, no. 1–2, pp. 142–149, Aug. 2018.

[26]   M. Xu, P. W. S. Heng, and C. V. Liew, "Formulation and process strategies to minimize coat damage for compaction of coated pellets in a rotary tablet press: A mechanistic view," *Int. J. Pharm.*, vol. 499, no. 1–2, pp. 29–37, Feb. 2016.

[27]   M. Dülle, H. Özcoban, and C. S. Leopold, "Analysis of the powder behavior and the residence time distribution within a production scale rotary tablet press," *Eur. J. Pharm. Sci.*, vol. 125, pp. 205–214, Dec. 2018.

[28]   M. Börner, A. Bück, and E. Tsotsas, "DEM-CFD investigation of particle residence time distribution in top-spray fluidised bed granulation," *Chem. Eng. Sci.*, vol. 161, pp. 187–197, 2017.

[29]   C. Wu, "DEM simulations of die filling during pharmaceutical tabletting," *Particuology*, vol. 6, pp. 412–418, 2008.

[30]   S. Schiano, L. Chen, and C.-Y. Wu, "The effect of dry granulation on flow behaviour of pharmaceutical powders during die filling," *Powder Technol.*, Sep. 2017.

[31]   Y. Guo and C.-Y. Wu, "Computational modeling of pharmaceutical die filling processes," *Predict. Model. Pharm. Unit Oper.*, pp. 253–271, Jan. 2017.

[32] M. S. Kadiri and A. Michrafy, "The effect of punch's shape on die compaction of pharmaceutical powders," *Powder Technol.*, vol. 239, pp. 467–477, May 2013.

[33] J. Kruisz, E. Faulhammer, J. Rehrl, O. Scheibelhofer, A. Witschnigg, and J. G. Khinast, "Residence time distribution of a continuously-operated capsule filling machine: Development of a measurement technique and comparison of three volume-reducing inserts," *Int. J. Pharm.*, vol. 550, no. 1–2, pp. 180–189, Oct. 2018.

[34] R. MacDonald, C. Reitmeier, R. MacDonald, and C. Reitmeier, "Food Processing," *Underst. Food Syst.*, pp. 179–225, Jan. 2017.

[35] S. V. James Malone, Aaron Totemeier, Norton Shapiro, "Lightbridge Corporation's Advanced Metallic Fuel for Light Water Reactors," *Nucl. Technol.*, vol. 180, no. 3, pp. 437–442.

[36] M. Kushner, "Nuclear Fuel Fabrication for Commercial Electric Power Generation," *IEEE Trans. Power Appar. Syst.*, vol. PAS-93, no. 1, pp. 244–247, Jan. 1974.

[37] Mitsubishi Nuclear Fuel, "Manufacturing Process in Tokai Plant (PWR Fuel)." .

[38] E. Supko, "Nuclear fuel fabrication," *Uranium Nucl. Power*, pp. 353–382, Jan. 2016.

[39] M. Liu, Y. Shao, and B. Liu, "Pressure analysis in the fabrication process of TRISO UO2-coated fuel particle," *Nucl. Eng. Des.*, vol. 250, pp. 277–283, Sep. 2012.

[40] W. Zhou, R. Liu, and S. T. Revankar, "Fabrication methods and thermal hydraulics analysis of enhanced thermal conductivity UO2–BeO fuel in light water reactors," *Ann. Nucl. Energy*, vol. 81, pp. 240–248, Jul. 2015.

[41] B. Van Snick *et al.*, "Impact of blend properties on die filling during tableting," *Int. J. Pharm.*, vol. 549, no. 1–2, pp. 476–488, Oct. 2018.

[42] H. P. Goh, P. W. S. Heng, and C. V. Liew, "Investigation on the impact of powder arching in small die filling," *Int. J. Pharm.*, vol. 551, no. 1–2, pp. 42–51, Nov. 2018.

[43] Z. Li, Y. Tang, X. Ding, C. Li, D. Yuan, and Y. Lu, "Reconstruction and thermal performance analysis of die-bonding filling states for high-power light-emitting diode devices," *Appl. Therm. Eng.*, vol. 65, no. 1–2, pp. 236–245, Apr. 2014.

[44] C.-Y. Wu and A. C. F. Cocks, "Flow behaviour of powders during die filling," *Powder Metall.*, vol. 47, no. 2, pp. 127–136, 2004.

[45] C.-Y. Wu and Y. Guo, "Numerical modelling of suction filling using DEM/CFD," *Chem. Eng. Sci.*, vol. 73, pp. 231–238, May 2012.

[46] N. Alberti, L. Cannizzaro, L. D'Acquisto, E. Lo Valvo, and F. Micari, "Computer-Aided Simulation of Die Filling Processes," *CIRP Ann.*, vol. 38, no. 1, pp. 239–242, Jan. 1989.

[47] P. A. Cundall and O. D. L. Strack, "A discrete numerical model for granular assemblies," *Géotechnique*, vol. 29, no. 1, pp. 47–65, 1979.

[48] K. Washino, E. L. Chan, K. Miyazaki, T. Tsuji, and T. Tanaka, "Time step criteria in DEM simulation of wet particles in viscosity dominant systems," *Powder Technol.*, vol. 302, pp. 100–107, 2016.

[49] R. Furukawa *et al.*, "Size-induced segregation during pharmaceutical particle die filling assessed by response surface methodology using discrete element method," *J. Drug Deliv. Sci. Technol.*, vol. 35, pp. 284–293, Oct. 2016.

[50] Y. Guo, C. Wu, K. D. Kafui, and C. Thornton, "3D DEM / CFD analysis of size-induced segregation during die filling," *Powder Technol.*, vol. 206, no. 1–2, pp. 177–188, 2011.

[51] O. C. Scheffler, C. J. Coetzee, and U. L. Opara, "A discrete element model (DEM) for predicting apple damage during handling," *Biosyst. Eng.*, vol. 172, pp. 29–48, Aug. 2018.

[52] M. Van Zeebroeck *et al.*, "The discrete element method (DEM) to simulate fruit impact damage during transport and handling: Model building and validation of DEM to predict bruise damage of apples," *Postharvest Biol. Technol.*, vol. 41, no. 1, pp. 85–91, Jul. 2006.

[53] Y. Tsuji, T. Kawaguchi, and T. Tanaka, "Discrete particle simulation of two-dimensional fluidized bed," *Powder Technol.*, vol. 77, no. 1, pp. 79–87, Oct. 1993.

[54] T. B. Anderson and R. Jackson, "Fluid Mechanical Description of Fluidized Beds. Equations of Motion," *Ind. Eng. Chem. Fundam.*, vol. 6, no. 4, pp. 527–539, Nov. 1967.

[55] T. Kawaguchi, T. Tanaka, and Y. Tsuji, "Numerical simulation of two-dimensional fluidized beds using the discrete element method (comparison between the two- and three-dimensional models)," *Powder Technol.*, vol. 96, no. 2, pp. 129–138, May 1998.

[56] L. Xu, K. Luo, Y. Zhao, J. Fan, and K. Cen, "Multiscale investigation of tube erosion in fluidized bed based on CFD-DEM simulation," *Chem. Eng. Sci.*, vol. 183, pp. 60–74, Jun. 2018.

[57] K. Kerst *et al.*, "CFD-DEM simulations of a fluidized bed crystallizer," 2017.

[58] H. A. Khawaja, "Sound waves in fluidized bed using CFD–DEM simulations," *Particuology*, vol. 38, pp. 126–133, Jun. 2018.

[59] W. R. Ketterhagen and B. C. Hancock, "Optimizing the design of eccentric feed hoppers for tablet presses using DEM," *Comput. Chem. Eng.*, vol. 34, no. 7, pp. 1072–1081, Jul. 2010.

[60] K. Mao, M. Y. Wang, Z. Xu, and T. Chen, "DEM simulation of particle damping," *Powder Technol.*, vol. 142, no. 2–3, pp. 154–165, Apr. 2004.

[61] A. Smith, C. James, R. Jones, P. Langston, E. Lester, and J. Drury, "Modelling contra-flow in crowd dynamics DEM simulation," *Saf. Sci.*, vol. 47, no. 3, pp. 395–404, Mar. 2009.

[62] L. QIU and C. WU, "A hybrid DEM/CFD approach for solid-liquid flows," *J. Hydrodyn. Ser. B*, vol. 26, no. 1, pp. 19–25, Feb. 2014.

[63] S. Natsui, S. Ueda, H. Nogami, J. Kano, R. Inoue, and T. Ariyama, "Gas–solid flow simulation of fines clogging a packed bed using DEM–CFD," *Chem. Eng. Sci.*, vol. 71, pp. 274–282, Mar. 2012.

[64] R. Mohanty, S. Mohanty, and B. K. Mishra, "Study of flow through a packed bed using discrete element method and computational fluid dynamics," *J. Taiwan Inst. Chem. Eng.*, vol. 63, pp. 71–80, Jun. 2016.

[65] H. Zhou, B. Yan, and Y. Zhang, "3D filling simulation of injection molding based on the PG method," *J. Mater. Process. Technol.*, vol. 204, no. 1–3, pp. 475–480, Aug. 2008.

[66] L. A. Mills and I. C. Sinka, "Effect of particle size and density on the die fill of powders," *Eur. J. Pharm. Biopharm.*, vol. 84, no. 3, pp. 642–652, Aug. 2013.

[67] P. W. Cleary and J. Ha, "Three-dimensional smoothed particle hydrodynamics simulation of high pressure die casting of light metal components," *J. Light Met.*, vol. 2, no. 3, pp. 169–183, Aug. 2002.

[68] C. Bierwisch, T. Kraft, H. Riedel, and M. Moseler, "Three-dimensional discrete element models for the granular statics and dynamics of powders in cavity filling," *J. Mech. Phys. Solids*, vol. 57, no. 1, pp. 10–31, Jan. 2009.

[69] T. Altan and V. Vazquez, "Status of process simulation using 2D and 3D finite element method 'What is practical today? What can we expect in the future?,'" *J. Mater. Process. Technol.*, vol. 71, no. 1, pp. 49–63, Nov. 1997.

[70] J. Capecelatro and O. Desjardins, "An Euler–Lagrange strategy for simulating particle-laden flows," *J. Comput. Phys.*, vol. 238, pp. 1–31, Apr. 2013.

[71] N. A. Patankar and D. D. Joseph, "Modeling and numerical simulation of particulate flows by the Eulerian-Lagrangian approach," *Int. J. Multiph. Flow*, vol. 27, no. 10, pp. 1659–1684, Oct. 2001.

[72] R. Garg, C. Narayanan, D. Lakehal, and S. Subramaniam, "Accurate numerical estimation of interphase momentum transfer in Lagrangian–Eulerian simulations of dispersed two-phase flows," *Int. J. Multiph. Flow*, vol. 33, no. 12, pp. 1337–1364, Dec. 2007.

[73] W. D. Fullmer and J. Musser, "CFD-DEM solution verification: Fixed-bed studies," *Powder Technol.*, vol. 339, pp. 760–764, Nov. 2018.

[74] R.-H. Wang, Q.-J. Guo, C.-G. Zhu, and C.-J. Li, "Multivariate spline approximation of the signed distance function," *J. Comput. Appl. Math.*, vol. 265, pp. 276–289, Aug. 2014.

[75] Y. Zhou, W. Zhang, J. Zhu, and Z. Xu, "Feature-driven topology optimization method with signed distance function," *Comput. Methods Appl. Mech. Eng.*, vol. 310, pp. 1–32, Oct. 2016.

[76] C. V. Deutsch and B. J. Wilde, "Modeling multiple coal seams using signed distance functions and global kriging," *Int. J. Coal Geol.*, vol. 112, pp. 87–93, Jun. 2013.

[77] J. H. Lim, H. Kim, S.-W. Kim, and D. Sohn, "A microstructure modeling scheme for unidirectional composites using signed distance function based boundary smoothing and element trimming," *Adv. Eng. Softw.*, vol. 109, pp. 1–14, Jul. 2017.

[78] G. Basinskas and M. Sakai, "Numerical study of the mixing efficiency of a ribbon mixer using the discrete element method," *Powder Technol.*, vol. 287, pp. 380–394, Jan. 2016.

[79] M. Sakai, Y. Shigeto, G. Basinskas, A. Hosokawa, and M. Fuji, "Discrete element simulation for the evaluation of solid mixing in an industrial blender," *Chem. Eng. J.*, vol. 279, pp. 821–839, Nov. 2015.

[80] Y. Tsunazawa, Y. Shigeto, C. Tokoro, and M. Sakai, "Numerical simulation of industrial die filling using the discrete element method," *Chem. Eng. Sci.*, vol. 138, pp. 791–809, Dec. 2015.

[81] C. G. Kang, P. K. Seo, and S. W. Youn, "Finite element analysis of thixoforming process with arbitrary shape die," *J. Mater. Process. Technol.*, vol. 159, no. 3, pp. 321–329, Feb. 2005.

[82] Y. Miyake, K. Tsujimoto, and H. Beppu, "Direct numerical simulation of a turbulent flow in a channel having periodic pressure gradient," *Int. J. Heat Fluid Flow*, vol. 16, no. 5, pp. 333–340, Oct. 1995.

[83] R. W. C. P. Verstappen and A. E. P. Veldman, "Direct numerical simulation of turbulence on a Connection Machine CM-5," *Appl. Numer. Math.*, vol. 19, no. 1–2, pp. 147–158, Nov. 1995.

[84] G. N. Coleman, J. Kim, and P. R. Spalart, "Direct numerical simulation of strained three-dimensional wall-bounded flows," *Exp. Therm. Fluid Sci.*, vol. 13, no. 3, pp. 239–251, Oct. 1996.

[85] G. Tryggvason, A. Esmaeeli, and N. Al-Rawahi, "Direct numerical simulations of flows with phase change," *Comput. Struct.*, vol. 83, no. 6–7, pp. 445–453, Feb. 2005.

[86] C. Xu and Z. Zhang, "The direct numerical simulation of a turbulent channel flow with analyses of the database," *Commun. Nonlinear Sci. Numer. Simul.*, vol. 1, no. 2, pp. 46–51, Apr. 1996.

[87] S. Solbakken and H. I. Andersson, "Direct numerical simulation of lubricated channel flow," *Fluid Dyn. Res.*, vol. 37, no. 3, pp. 203–230, Sep. 2005.

[88] D. Deising, D. Bothe, and H. Marschall, "Direct numerical simulation of mass transfer in bubbly flows," *Comput. Fluids*, vol. 172, pp. 524–537, Aug. 2018.

[89] X. Feng, C. Yang, Z.-S. Mao, J. Lu, and G. Tryggvason, "Bubble induced turbulence model improved by direct numerical simulation of bubbly flow," *Chem. Eng. J.*, Sep. 2018.

[90] J. H. Kim and J. H. Lee, "Direct numerical simulation of a turbulent Couette–Poiseuille flow: Turbulent statistics," *Int. J. Heat Fluid Flow*, vol. 72, pp. 288–303, Aug. 2018.

[91] H. Zhao, A. Wei, K. Luo, and J. Fan, "Direct numerical simulation of turbulent boundary layer with heat transfer," *Int. J. Heat Mass Transf.*, vol. 99, pp. 10–19, Aug. 2016.

[92] S. H. Kang, "Direct numerical simulation of the turbulent premixed flame propagation with radiation effects," *Int. J. Heat Mass Transf.*, vol. 102, pp. 323–330, Nov. 2016.

[93] T. Dairay and J. C. Vassilicos, "Direct numerical simulation of a turbulent wake: The non-equilibrium dissipation law," *Int. J. Heat Fluid Flow*, vol. 62, pp. 68–74, Dec. 2016.

[94] E. Ghasemi, H. Bararnia, S. Soleimanikutanaei, and C. X. Lin, "Direct numerical simulation and analytical modeling of electrically induced multiphase flow," *Int. J. Mech. Sci.*, vol. 142–143, pp. 397–406, Jul. 2018.

[95] G. Tryggvason, A. Esmaeeli, J. Lu, and S. Biswas, "Direct numerical simulations of gas/liquid multiphase flows," *Fluid Dyn. Res.*, vol. 38, no. 9, pp. 660–681, Sep. 2006.

[96] L. Schneiders, D. Hartmann, M. Meinke, and W. Schröder, "An accurate moving boundary formulation in cut-cell methods," *J. Comput. Phys.*, vol. 235, pp. 786–809, Feb. 2013.

[97] G. Rosatti, D. Cesari, and L. Bonaventura, "Semi-implicit, semi-Lagrangian modelling for environmental problems on staggered Cartesian grids with cut cells," *J. Comput. Phys.*, vol. 204, no. 1, pp. 353–377, Mar. 2005.

[98] M. Berger, "A note on the stability of cut cells and cell merging," *Appl. Numer. Math.*, vol. 96, pp. 180–186, Oct. 2015.

[99] N. Gokhale, N. Nikiforakis, and R. Klein, "A dimensionally split Cartesian cut cell method for hyperbolic conservation laws," *J. Comput. Phys.*, vol. 364, pp. 186–208, Jul. 2018.

[100] W. P. Bennett, N. Nikiforakis, and R. Klein, "A moving boundary flux stabilization method for Cartesian cut-cell grids using directional operator splitting," *J. Comput. Phys.*, vol. 368, pp. 333–358, Sep. 2018.

[101] C. S. Peskin, "Numerical analysis of blood flow in the heart," *J. Comput. Phys.*, vol. 25, no. 3, pp. 220–252, Nov. 1977.

[102] X. Sun and M. Sakai, "Immersed Boundary Method with Artificial Density in Pressure Equation for Modeling Flows Confined by Wall Boundaries," *J. Chem. Eng. Japan*, vol. 50, no. 3, pp. 161–169, 2017.

[103] Y. YUKI, S. TAKEUCHI, and T. KAJISHIMA, "Efficient Immersed Boundary Method for Strong Interaction Problem of Arbitrary Shape Object with the Self-Induced Flow," *J. Fluid Sci. Technol.*, vol. 2, no. 1, pp. 1–11, 2007.

[104] T. Kajishima, S. Takiguchi, H. Hamasaki, and Y. Miyake, "Turbulence Structure of Particle-Laden Flow in a Vertical Plane Channel Due to Vortex Shedding," *JSME Int. J. Ser. B Fluids Therm. Eng.*, vol. 44, no. 4, pp. 526–535, 2001.

[105] C. Chen, "Investigations on Mesoscale Structure in Gas–Solid Fluidization and Heterogeneous Drag Model," in *Investigations on Mesoscale Structure in Gas–Solid Fluidization and Heterogeneous Drag Model*, 1st ed., Springer-Verlag Berlin Heidelberg, 2016, pp. 33–53.

[106] W. Wang and J. Li, "Simulation of gas-solid two-phase flow by a multi-scale CFD approach-of the EMMS model to the sub-grid level," *Chem. Eng. Sci.*, vol. 62, no. 1–2, pp. 208–231, 2007.

81

[107] L. Lu, J. Xu, W. Ge, Y. Yue, X. Liu, and J. Li, "EMMS-based discrete particle method (EMMS-DPM) for simulation of gas-solid flows," *Chem. Eng. Sci.*, vol. 120, pp. 67–87, 2014.

[108] X. Qiu, L. Wang, N. Yang, and J. Li, "A simplified two-fluid model coupled with EMMS drag for gas-solid flows," *Powder Technol.*, vol. 314, pp. 299–314, Jun. 2017.

[109] C. Li and A. Strachan, "Coarse-grained molecular dynamics modeling of reaction-induced phase separation," *Polymer (Guildf).*, vol. 149, pp. 30–38, Aug. 2018.

[110] D. Queteschiner, T. Lichtenegger, S. Pirker, and S. Schneiderbauer, "Multi-level coarse-grain model of the DEM," *Powder Technol.*, vol. 338, pp. 614–624, Oct. 2018.

[111] L. M. C. Sagis, "Coarse-grained models for diffusion in oil-filled hydrogel microbeads," *Food Hydrocoll.*, vol. 89, pp. 294–301, Apr. 2019.

[112] M. Sakai and S. Koshizuka, "Large-scale discrete element modeling in pneumatic conveying," *Chem. Eng. Sci.*, vol. 64, no. 3, pp. 533–539, Feb. 2009.

[113] M. Sakai *et al.*, "Verification and validation of a coarse grain model of the DEM in a bubbling fluidized bed," *Chem. Eng. J.*, vol. 244, pp. 33–43, May 2014.

[114] H. Yao, Y. Mori, K. Takabatake, X. Sun, and M. Sakai, "Numerical investigation on the influence of air flow in a die filling process," *J. Taiwan Inst. Chem. Eng.*, vol. 90, pp. 9–17, Dec. 2018.

[115] S. Ergun, "Fluid flow through packed columns," *Chem. Eng. Progr.*, vol. 48, pp. 89–94, 1952.

[116] C. Y. Wen and Y. H. Yu, "Mechanics of fluidization," *Chem. Eng. Progress, Symp. Ser.*, vol. 62, no. 1, pp. 100–111, 1966.

[117] J. N. Israelachvili, *Intermolecular and Surface Forces*, Third edit. Waltham, MA, USA: Academic Press, 2011.

[118] G. Lomboy, S. Sundararajan, K. Wang, and S. Subramaniam, "A test method for determining adhesion forces and Hamaker constants of cementitious materials using atomic force microscopy," *Cem. Concr. Res.*, vol. 41, no. 11, pp. 1157–1166, Nov. 2011.

[119] T. B. Anderson and R. O. Y. Jackson, "A Fluid Mechanical Description of Fluidized Beds," *Ind. Eng. Chem. Fundam.*, vol. 6, no. 4, pp. 527–539, 1967.

[120] W. M. H. K. Versteeg, *An Introduction to Computational Fluid Dynamics The Finite Volume Method*, Second. Edinburgh: Pearson Education Limited, 2007.